Title

Hypoxia induces adrenomedullin from lung epithelia, stimulating ILC2 inflammation and immunity.

Journal

Journal of Experimental Medicine, 219(6)

Authors

Han, Jihye
Wan, Qingqing
Seo, Goo-Young
et al.

Publication Date

2022-06-06

DOI

10.1084/jem.20211985

Peer reviewed

JEM Journal of Experimental Medicine

ARTICLE

Hypoxia induces adrenomedullin from lung epithelia, stimulating ILC2 inflammation and immunity

Jihye Han[1], Qingqing Wan[1,3], Goo-Young Seo[1], Kenneth Kim[1], Sarah el Baghdady[1], Jee H. Lee[1], Mitchell Kronenberg[1,2], and Yun-Cai Liu[1,3]

Hypoxia contributes to airway inflammation and remodeling in several lung diseases; however, exactly how hypoxic pulmonary epithelium regulates allergic inflammation remains to be fully characterized. Here, we report that conditional deletion of the E3 ubiquitin ligase VHL in lung epithelial cells resulted in exacerbated type 2 responses accompanied by selective increase of group 2 innate lymphoid cells (ILC2s) at steady state and following inflammation or helminth infection. Ablation of expression of the hypoxia-inducible factor 2α (HIF2α) significantly reversed VHL-mediated ILC2 activation. VHL deficiency in lung epithelial cells caused increased expression of the peptide hormone adrenomedullin (ADM), and our data suggest that HIF2α controls *Adm* expression. ADM directly promoted ILC2 activation both in vitro and in vivo. Our findings indicate that the hypoxic response mediated by the VHL–HIF2α axis is critical for control of pulmonary type 2 responses by increasing ADM expression in lung epithelia, causing ILC2 activation.

Introduction

Type 2 immunity controls diverse homeostatic and immune processes in health and disease, including the responses to metazoan parasites as well as the induction of pathogenic conditions, such as allergic asthma, allergic rhinitis, atopic dermatitis, and anaphylaxis. The type 2 inflammatory responses are induced by exposure to various infectious and environmental stimuli, such as allergens, helminth infections, venoms, and other triggers (Hammad and Lambrecht, 2015; Palm et al., 2012). Several types of lymphocytes are involved in this response, including $CD4^+$ T helper type 2 cells (Th2), innate-like T cells such as invariant natural killer T cells, and type 2 innate lymphoid cells (ILC2s), leading to the release of type 2 cytokines such as IL-4, IL-5, and IL-13. These cytokines cause IgE production, tissue eosinophilia, mucus production by goblet cells, and airway hyperresponsiveness. The initiation of type 2 immune responses is known to be triggered by cross-talk between innate immune cells and epithelium at mucosal sites such as skin, lung, and intestine (Palm et al., 2012; Pulendran and Artis, 2012).

The pulmonary epithelium is a first line of defense against inhaled environmental challenges and is indispensable for normal gas exchange. Epithelial cells lining the lung act as a physical and chemical barrier. They secrete mucus and other host defense molecules into the mucosa in response to external stimuli to protect the lungs from infection and injury (Rackley and Stripp, 2012). Airway epithelial damage by allergens or inhaled pathogens causes epithelial secretion of alarmins including IL-25, IL-33, and thymic stromal lymphopoietin (TSLP). These cytokines elicit the release of type 2 effector cytokines from innate and adaptive immune cells, which leads to diverse immune responses ranging from anti-helminth immunity to allergic inflammation, tissue remodeling, and even pathological pulmonary fibrosis (Hammad and Lambrecht, 2015; Roan et al., 2019; Whitsett and Alenghat, 2015).

Recent studies revealed a role for ILC2s in the initiation and amplification of allergic responses. ILC2s have both common features and differences compared with Th2 cells. Notably, ILC2s and Th2 cells both express the transcription factor GATA3 and share cytokine profiles, including synthesis of IL-4, IL-5, IL-9, IL-13, and amphiregulin (Zaiss et al., 2015). In contrast to Th2 cells, which require cytokine polarization that is induced after infection, at steady state, ILC2s are enriched at the mucosal surface and rapidly respond to local alarmins by generating large amounts of type 2 cytokines (Artis and Spits, 2015). Emerging evidence indicates that a range of microenvironmental factors besides alarmins positively or negatively regulate effector functions of ILC2s. These include cytokines, hormones, neuropeptides, lipid mediators, and costimulatory molecules (Hurrell et al., 2018; Klose and Artis, 2016). However, pulmonary

[1]La Jolla Institute for Immunology, La Jolla, CA; [2]Division of Biological Sciences, University of California San Diego, La Jolla, CA; [3]Institute for Immunology, Tsinghua-Peking Center for Life Sciences, School of Medicine, Tsinghua University, Beijing, China.

Correspondence to Mitchell Kronenberg: mitch@lji.org; Yun-Cai Liu: yuncail@hotmail.com; Jihye Han: jhan@lji.org.

epithelium-derived factors that regulate ILC2 effector functions still need to be characterized.

Lung inflammation results in hypoxic responses and the accumulation of hypoxia-inducible factors (HIFs), which in turn drives chronic inflammatory lung diseases such as asthma, chronic obstructive pulmonary disease (COPD), and pulmonary fibrosis (Darby and Hewitson, 2016; Lee et al., 2019). The HIFs regulate transcriptional responses to hypoxia. They are heterodimeric transcription factors comprising a hypoxia-sensitive α subunit (HIF1α, HIF2α, and HIF3α) and a constitutively expressed β subunit (HIFβ). Under normoxic conditions, HIFs are rapidly degraded via the hydroxylation by prolyl hydroxylase domain enzymes (PHDs), leading to recognition by the von Hippel–Lindau (VHL) E3 ubiquitin ligase complex, followed by proteasomal degradation. On the other hand, hypoxia reduces the activity of PHD enzymes, which stabilizes HIFα. Stabilized HIFα proteins translocate into the nucleus, where they heterodimerize with HIFβ and then bind to the hypoxia-responsive elements (HREs) of target genes, resulting in initiation of HIF-dependent transcriptional programs (Lee et al., 2019; Schofield and Ratcliffe, 2004).

Previous studies have shown critical roles of HIFs in lung immune responses. For example, hypoxia leads to pathogenic fibrosis by inducing vascular remodeling, extracellular matrix accumulation, and epithelial-to-mesenchymal transition via HIF-dependent mechanisms (Goodwin et al., 2018; Higgins et al., 2007; Tzouvelekis et al., 2007). Whereas previous reports suggest possible roles of VHL–HIF pathways in the lung immune response, it is still unknown if the VHL–HIF axis is involved in controlling type 2 inflammation by modulating epithelial function. To address this question, we generated epithelial cell–specific VHL-deficient mice and showed increased lung type 2 inflammation. We further showed that a HIF2α-driven transcriptional program in bronchiolar epithelial cells increased the expression of adrenomedullin (ADM), a protein important for a variety of physiologic processes including vasodilation, and directly potentiated pulmonary ILC2s. Collectively, our study results indicate that the VHL–HIF2α axis plays an important role in controlling pulmonary type 2 responses through the regulation of cross talk between epithelial cells and ILC2s.

Results

VHL deletion in lung epithelial cells leads to chronic inflammation

To determine whether lung inflammation results in hypoxic responses and the accumulation of HIF proteins in epithelial cells and whole lung tissue, we used papain- and bleomycin-induced airway inflammation models. We found that both papain- and bleomycin-treated lungs had higher levels of stabilized HIF proteins by Western blot (Fig. S1 A) than PBS-treated control lungs. When total epithelial cells were analyzed by flow cytometry, HIF1α was increased in both models and HIF2α in the bleomycin model (Fig. 1, A and B). We administered pimonidazole hydrochloride, which is reductively activated and leads to stable adducts with intracellular biomolecules in hypoxic cells, to visualize hypoxic tissue regions in vivo. Immunoblotting revealed that hypoxic adducts were observed in the lungs of challenged mice (Fig. S1 A). By immunofluorescence analysis, we detected hypoxic areas in both the interstitial regions and bronchiolar epithelium from the lungs with either papain or bleomycin challenge (Fig. 1 C). We also infected control mice with parasitic helminth *Nippostrongylus brasiliensis* (*N.b.*), and the results showed that *N.b.* infection induced the transcription of hypoxia-related genes in whole lung tissue (Fig. S1 B). These data suggested that a hypoxic microenvironment was induced in mouse models of lung inflammation.

Because of the role of epithelial cells in lung inflammation (Rackley and Stripp, 2012) and the prominent epithelial staining with pimonidazole hydrochloride, we investigated the role of HIF stabilization in epithelial cells. To this end, we generated $Vhl^{fl/fl}$*Cc10*-Cre conditional knockout (cKO) mice and analyzed the lungs of young mice (8–12 wk of age) at steady state. CC10, also known as clara cell secretory protein (CCSP), is expressed in club cells, which are present in the pulmonary distal bronchial/bronchiolar epithelium in both mice and humans. Their primary function is production of immunomodulatory proteins, including secretory surfactants and other cytokines (Rokicki et al., 2016). We found that VHL cKO mice had poorly collapsed lungs with multifocal to coalescing petechiae by 8 wk of age (Fig. 1 D). Cytologic, flow cytometric, and histopathologic analyses demonstrated increased numbers of erythrocytes and total nucleated cells in bronchiolar alveolar lavage (BAL) and lung tissues compared with WT control mice. In addition, VHL cKO mice displayed mild inflammation, but with significant increases of inflammatory cells including lymphocytes, eosinophils, and neutrophils in the BAL fluid as well as in the lung (Fig. 1, E and F). However, further detailed analysis of $CD4^+$ T cells in the lung and mediastinal lymph node (mLN) revealed that there were no differences in their numbers between WT and cKO mice, except that VHL cKO showed increased IL-13^+CD4^+ T cells in the lung compared with WT mice (Fig. S1, C and D). Accompanied with the increased cell populations, VHL cKO mice showed mild perivascular inflammation and moderate alveolar hemorrhage at 8 wk of age; however, they showed increasing features of severe hemorrhage, thrombosis, and chronic type 2 inflammation by 9 mo. Aged VHL cKO mice spontaneously displayed hemorrhage and immune cell infiltration, with more severely damaged lung tissue (Fig. 1 G). To further study the details of the enhanced type 2 immunity in VHL cKO mice, we examined the expression of type 2–related genes from whole lung extracts. VHL-deficient mice showed higher amounts of mRNAs encoding type 2–related cytokines and chemokines, including IL-33, IL-5, IL-13, and other factors, such as *Relma*, associated with type 2 immunity (Fig. S1 E). Together, these data indicated that VHL deficiency resulted in chronic type 2 inflammation in the lung under resting conditions.

VHL deficiency results in selective increase of ILC2s

ILC2s are considered important initiators of type 2 immunity (Artis and Spits, 2015). Therefore, we examined by flow cytometry whether VHL deletion in lung epithelial cells affected ILC2s. VHL deficiency resulted in increased ILC2s and a

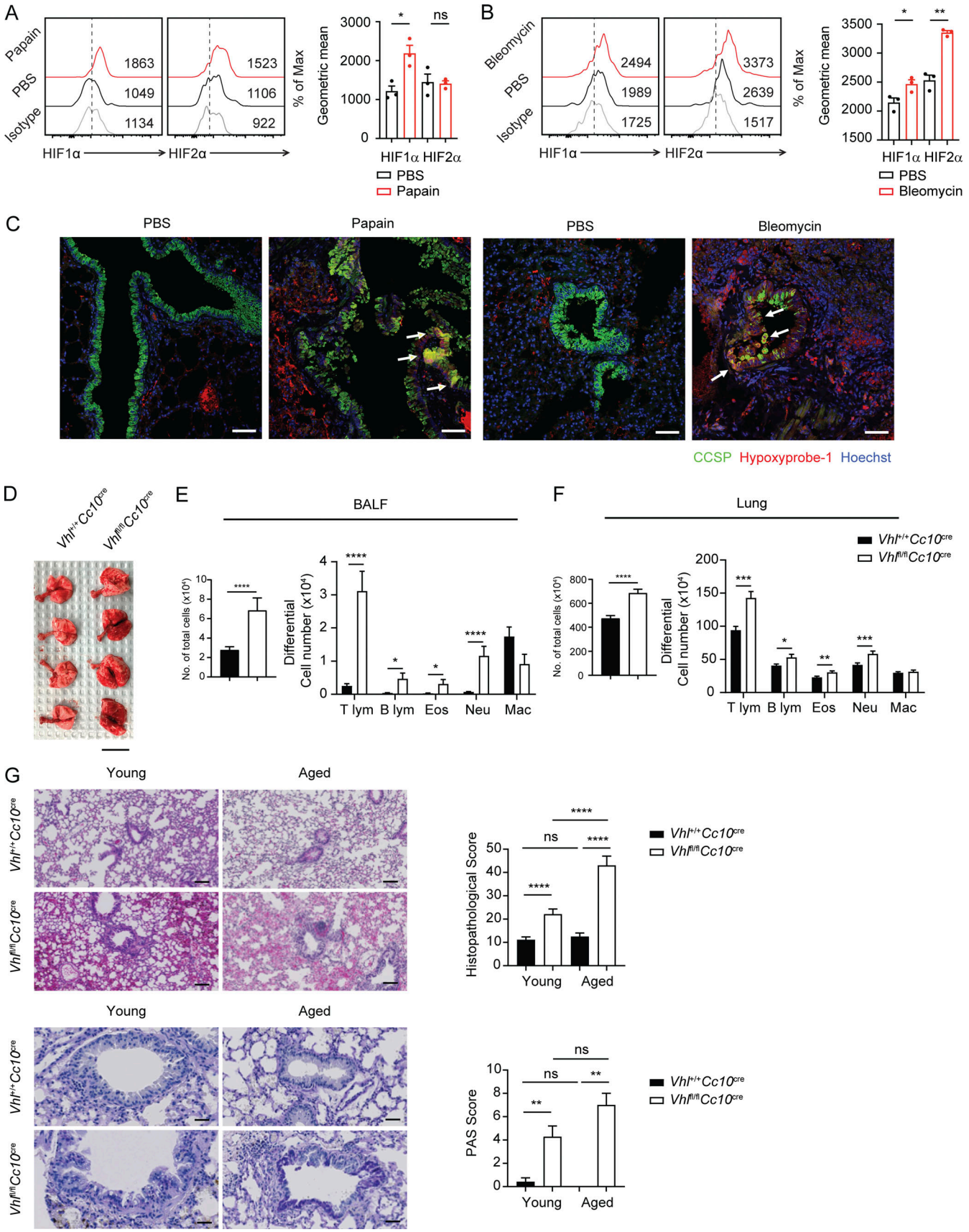

Figure 1. **Mice lacking epithelial VHL develop chronic lung inflammation. (A and B)** Representative data show HIF1α and HIF2α expression in bronchiolar epithelial cells from C57BL/6 mice after papain (A) and bleomycin (B) challenge. Mean fluorescence intensity (MFI) was measured by flow cytometry. *, P <

0.05; **, P < 0.01 (Student's *t* test). **(C)** Representative section of the lungs stained for CCSP (green), hypoxyprobe-1 (red), and Hoechst (blue); 20× magnification; scale bar, 50 µm. White arrows highlight epithelial cells that show hypoxia. **(A–C)** *n* = 2–3 mice/group. Data are representative of two independent experiments. **(D)** Images of lungs from 8–12-wk-old WT and VHL cKO mice. Scale bar, 2.54 cm. **(E and F)** The numbers of total cells and inflammatory cells from BALF (E) and lung (F). *n* = 3–5 mice/group, pooled from more than three independent experiments. *, P < 0.05; **, P < 0.01; ***, P < 0.001; ****, P < 0.0001 (Student's *t* test). **(G)** Histology of lung from WT and VHL cKO mice and histological score. The lung sections from young (≤12 wk old, left) and aged (9 mo old, right) mice were stained with H&E (upper row) and PAS (lower). Scale bars, 100 µm. **(G)** *n* = 2–3 aged mice pooled from two independent experiments and *n* = 3–5 young mice pooled from more than three independent experiments. *, P < 0.05; **, P < 0.01; ***, P < 0.001; ****, P < 0.0001 by one-way ANOVA followed by Tukey's test. All data presented as mean ± SEM.

proportional increase in the number of ILC2 cells that expressed the activation marker KLRG1 (Fig. 2, A and B). On a per-cell basis, we observed a moderate increase in the percentages of IL-5– and IL-5 plus IL-13–producing lung ILC2 cells in VHL cKO mice (Fig. 2, C and D). The main effect, however, was in the ILC2 cell numbers, without a similar increase in ILC1s and ILC3s (Fig. 2 E). To examine proliferation of ILC2s, we examined Ki-67 expression on ILC2s of WT and VHL cKO mice. We showed that ILC2s from VHL cKO mice at postnatal age 12–14 d expressed a higher level of Ki-67 compared with ILC2s of WT mice; however, 8–12-wk-old adult mice showed no difference in the rate of Ki67 expression in lung ILC2s. The data implied that active proliferation of ILC2s in the lung in young mice may result in increased ILC2s throughout adulthood (Fig. S1 F).

Inflammatory ILC2s (iILC2s) have high expression of the IL-25 receptor (IL-17RB) and KLRG1, but low expression of the IL-33 receptor (T1/ST2; Huang et al., 2015), in contrast to natural ILC2s (nILC2) at steady state at mucosal sites, which express high amounts of both KLRG1 and T1/ST2. To study if VHL deficiency affected the number of iILC2s, we analyzed the $ST2^{lo}KLRG1^{hi}$ population in $Lin^{-}CD90.2^{+}CD127^{+}$ ILCs. Whereas nILC2s were increased in VHL cKO mice in comparison with WT mice, the population of iILC2s was similar between control and cKO mice (Fig. 2 F). Taken together, these data demonstrated that VHL deficiency in lung epithelia selectively increased the number of ILC2s, but not other ILC subtypes.

VHL negatively regulates ILC2-mediated responses

To determine whether VHL deletion in bronchiolar epithelial cells affected type 2 immune responses, we used several model systems. In the papain-induced airway inflammation model (Fig. 3 A), papain proteolysis disrupts the integrity of airway epithelium, resulting in the release of alarmins, which subsequently activate ILC2s to induce eosinophilic inflammation (Halim et al., 2012). VHL deletion in club cells led to significantly increased ILC2 accumulation (Fig. 3 B), with enhanced airway eosinophilia (Fig. 3, C and D), after papain challenge. Although quantities of periodic acid–Schiff (PAS) staining mucin were similar in VHL WT and cKO groups, there was an increase of type 2 cells in VHL cKO mice that was also accompanied by histological changes, as revealed by hemorrhage and interstitial infiltration by eosinophils and other immune cells (Fig. 3 E). We confirmed a role for VHL in limiting lung inflammation by using a bleomycin-induced pulmonary injury model. VHL deficiency led to a selective increase in ILC2s (Fig. S2, A and B), which developed severe type 2–mediated immune responses in the lung and mLN compared with WT controls (Fig. S2, C and D).

ILC2s also play a critical and beneficial role in the lung during early phases of infection with the parasitic helminth *N.b.*, resulting in eosinophilic inflammation and helminth clearance (Price et al., 2010). Therefore, we infected mice with *N.b.* larvae, followed by analysis of inflammation in the lung and worm burden in the small intestine (Fig. 3 F). The numbers of ILC2s and KLRG1-expressing activated ILC2s were increased in both WT and VHL-deleted mice (Fig. 3 G). We observed an increase in the total numbers of IL-5 and/or IL-13 producing lung ILC2 cells in VHL cKO mice compared with control mice 2 d after *N.b.* infection (Fig. 3 H). Significant increases in both the percentage and the total numbers of eosinophils were observed in the lungs of infected VHL cKO mice compared with their WT counterparts (Fig. 3 I). In addition, intestinal worm burdens were significantly lower on day 7 after infection in VHL cKO mice (Fig. 3 J), suggesting that increased lung ILC2s in VHL cKO mice could play an important role in worm expulsion. Altogether, using model systems of induced inflammation and infection, these data demonstrated that VHL deficiency in lung epithelium enhanced ILC2-driven type 2 immune responses, which could be detrimental or beneficial, depending on the circumstances.

HIF2α contributes to VHL-mediated regulation of ILC2s

HIFα proteins are well-established targets for degradation by the VHL E3 ubiquitin ligase complex, and VHL deficiency results in the accumulation of HIFα proteins, including HIF1α and HIF2α (Schofield and Ratcliffe, 2004). To characterize HIFα expression in lung epithelium, we measured HIF1α and HIF2α proteins in bronchiolar epithelial cells by using flow cytometry. We confirmed increased accumulation of both HIF1α and HIF2α in VHL-deficient bronchiolar epithelial cells by flow cytometry (Fig. 4 A). We could not gate on CC10-expressing cells by flow cytometry, because of the lack of an appropriate antibody, and therefore by necessity only some epithelial cells were affected. $Hif1a^{fl/fl}Cc10^{cre}$ and $Hif2a^{fl/fl}Cc10^{cre}$ cKO mice served as a negative control, confirming that expression of HIF1α and HIF2α proteins accumulated in VHL-deficient bronchiolar epithelial cells (Fig. S3 A). In addition, quantitative real-time PCR (qPCR) data showed that the expression of glycolysis-related factors, known target genes of HIFα, were upregulated in VHL-deficient cells compared with WT controls (Fig. 4 B). Immunofluorescence analysis revealed that HIF1α accumulated only when VHL was deleted, whereas HIF2α was constitutively expressed on WT bronchiolar epithelial cells, but also was upregulated in VHL-deficient club cells (Fig. 4, C and D).

HIFα expression profiles were further examined by analyzing published single-cell RNA sequencing (RNA-seq) datasets from subpopulations of mouse tracheal epithelia (Montoro et al., 2018). We found that the genes encoding HIF2α were most highly expressed in $CCSP^{+}$ club cells and basal cells, whereas

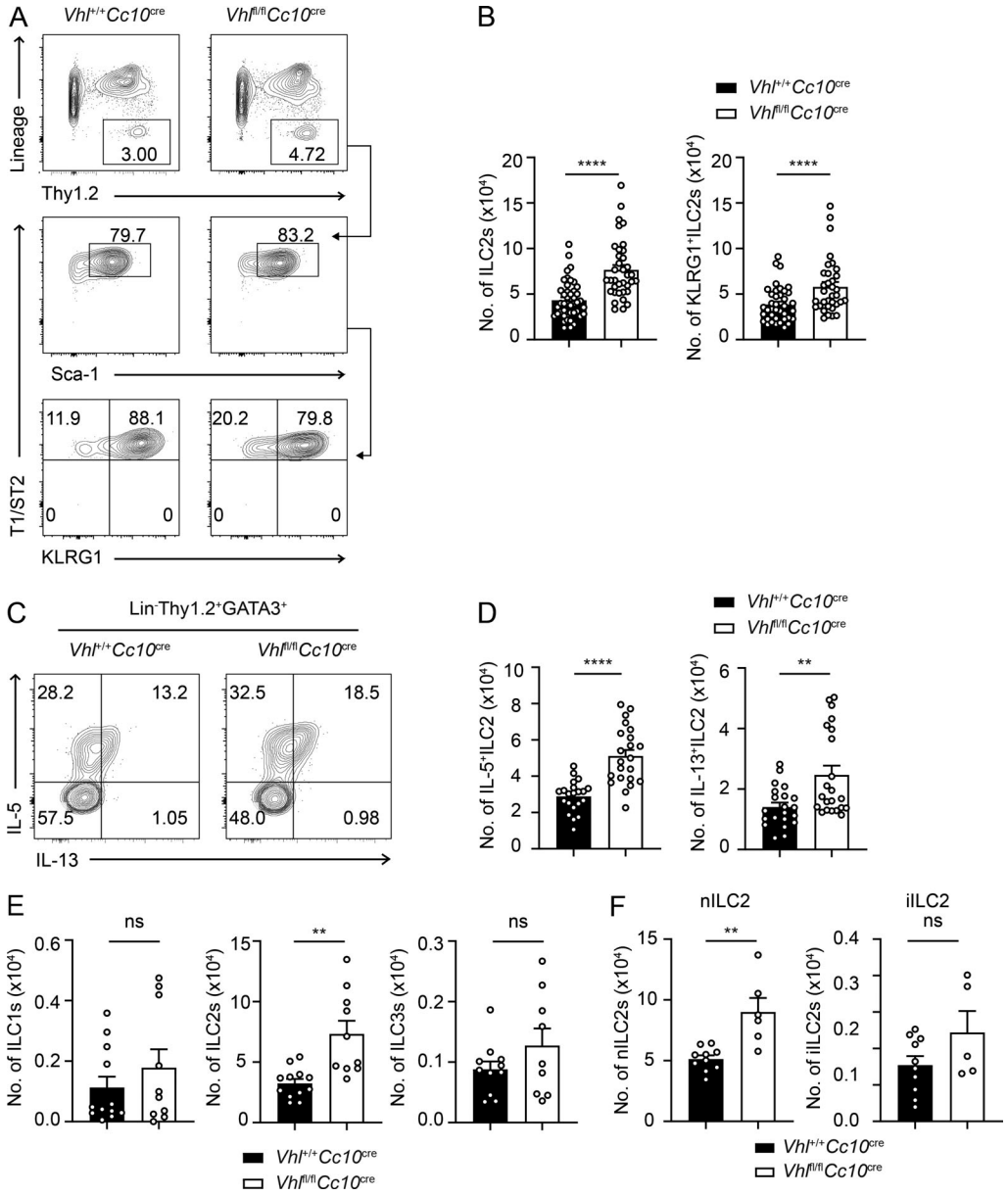

Figure 2. **VHL deficiency leads to selective increase of ILC2, but not other ILC subtypes. (A)** Gating strategy and cytometric analysis of ILC2s from lung in WT and VHL cKO mice. Lung ILC2s were identified as CD45$^+$Lin$^-$Thy1.2$^+$CD127$^+$CD25$^+$ST2$^+$Sca-1$^+$. Lineage-negative gating included antibodies for CD3, CD4, CD8, TCRβ, TCRγδ, NK1.1, CD11b, CD11c, B220, Ter119, and Gr-1. Numbers indicate the percentage of events. **(B)** Total numbers of lung ILC2s assessed in A. **(C)** Flow cytometric analysis of intracellular expression of IL-5 and IL-13 from Lin$^-$CD3$^-$Thy1.2$^+$GATA3$^+$ ILC2s in the lung stimulated with PMA and ionomycin. Lineage markers included CD11b, CD11c, CD19, NK1.1, B220, and Ter119. **(D)** Total numbers of IL-5$^+$ or IL-13$^+$ cells in lung ILC2s. **(E)** Total numbers of ILC1, ILC2, and ILC3 from WT and VHL cKO mice. **(F)** Total numbers of lung nILC2 and iILC2s in WT and VHL cKO mice. nILC2 assessed as CD45$^+$Lin$^-$Thy1.2$^+$ST2$^+$KLRG1$^+$; iILC2s assessed as CD45$^+$Lin$^-$Thy1.2$^+$ST2^{lo}KLRG1^{high}. **(B and D–F)** n = 3–5 mice/group pooled from more than three independent experiments. **, P < 0.01; ****, P < 0.0001 (Student's t test). All data presented as mean ± SEM.

HIF1α was barely expressed in tracheal epithelial subsets (Fig. S3 B). These data implied that HIF2α expression was abundant in bronchiolar club cells even under normal conditions and was increased by VHL deficiency.

To further identify whether HIF1α or HIF2α is mainly involved in potentiating ILC2 functions, we generated both *Vhl*$^{fl/fl}$ *Hif1a*$^{fl/fl}$*Cc10*-Cre double-knockout (VHL/HIF1α DKO) and *Vhl*$^{fl/fl}$ *Hif2a*$^{fl/fl}$*Cc10*-Cre double knockout (VHL/HIF2α DKO) mice and analyzed lung ILC2 populations. We found that VHL and HIF2α double deficiency reversed the enhanced ILC2 number and spontaneous eosinophilic inflammation observed in VHL single-deficient mice or after papain, whereas VHL and HIF1α double deficiency did not reverse changes under steady state (Fig. 4, E and F) or after papain challenge (Fig. 4, G and H). Taken together, these results demonstrated a critical role for the VHL–HIF2α axis in the regulation of bronchiolar epithelial function in pulmonary type 2 responses by regulating the number and function ILC2 cells.

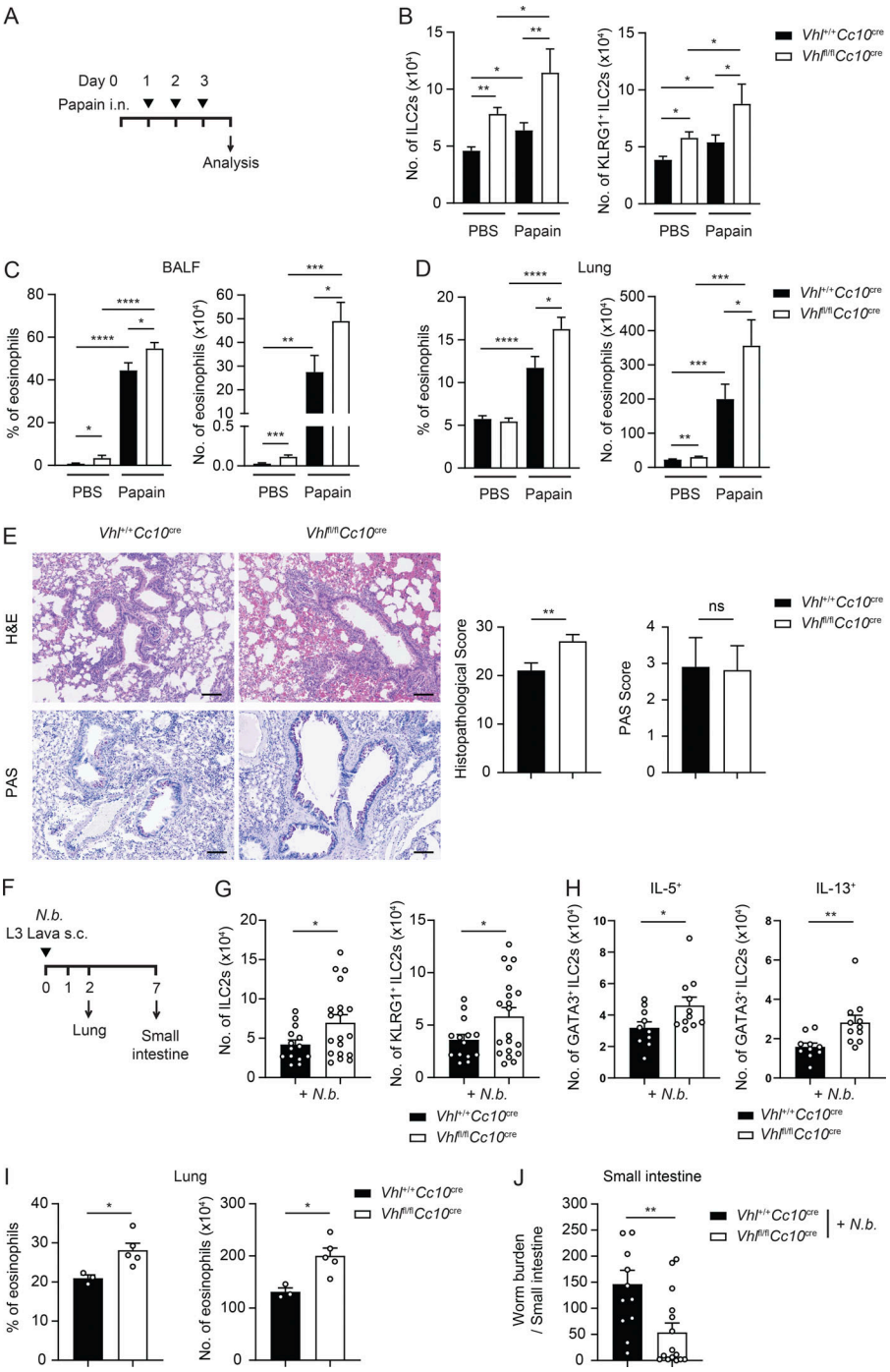

Figure 3. **VHL-deficient mice display severe inflammation upon allergic triggering. (A)** Experimental protocol for papain-induced airway inflammation model. **(B)** Total numbers of ILC2s and KLRG1⁺ ILC2. **(C and D)** Frequencies and total number of eosinophils (Eos; CD45⁺CD11c$^{-/lo}$SiglecF⁺) in BAL fluid (C) and lungs (D). *, P < 0.05; **, P < 0.01; ***, P < 0.001; ****, P < 0.0001 by one-way ANOVA followed by Tukey's test. **(E)** Histology of lung from WT and VHL cKO mice and histological score. Lung sections were stained with H&E and PAS. Scale bars, 50 µm. **(F)** Experimental protocol for nematode parasite *N.b.* infection. **(G)** Total numbers of ILC2s and KLRG1⁺ cells among total ILC2s. **(H)** The number of IL-5– or IL-13–secreting ILC2s was determined after 4-h stimulation with PMA and ionomycin. **(I)** Frequencies and total numbers of eosinophils from lung were determined by flow cytometry. **(J)** Worm burden in the small intestine 7 d after *N.b.* infection. **(E and G–J)** *n* = 3–5 mice/group pooled from three independent experiments. *, P < 0.05; **, P < 0.01 (Student's *t* test). All data presented as mean ± SEM.

VHL regulates the expression of epithelium-derived soluble factors

To explore whether VHL-deficient lung epithelial cells directly activated ILC2s, we generated a CRISPR-mediated VHL knockout in the C22 mouse club cell–like cell line (Fig. S3 C) and cocultured them with sorted ILC2s in vitro. VHL knockout in C22 club cells resulted in increased expression of hypoxia-related genes and accumulated HIFα proteins (Fig. S3, D–F). VHL KO-C22 cells effectively supported ILC2s in vitro more than control cells by facilitating ILC2 proliferation and the production of IL-5 and IL-13, in both the absence and the presence of exogeneous IL-7 and IL-33 (Fig. 4, I–K). These data suggested that VHL-deficient epithelial cells directly potentiated ILC2s.

To further identify epithelium-derived soluble factors responsible for the increased number of ILC2s in mice with VHL-deficient epithelial cells, we cultured ILC2s isolated from WT in vitro with BAL fluid–conditioned medium from the lungs of VHL cKO and WT mice. ILC2s cultured with VHL cKO-conditioned medium showed increased proliferation (Fig. 4 L), with enhanced production of effector cytokines compared with ILC2s cultured with WT-conditioned medium (Fig. 4, M and N). In addition, we found that the enhanced proliferation and cytokine production of ILC2s cultured with VHL cKO-conditioned medium were not observed when ILC2s were cultured with conditioned medium from VHL/HIF2α DKO mice (Fig. 4, L–N).

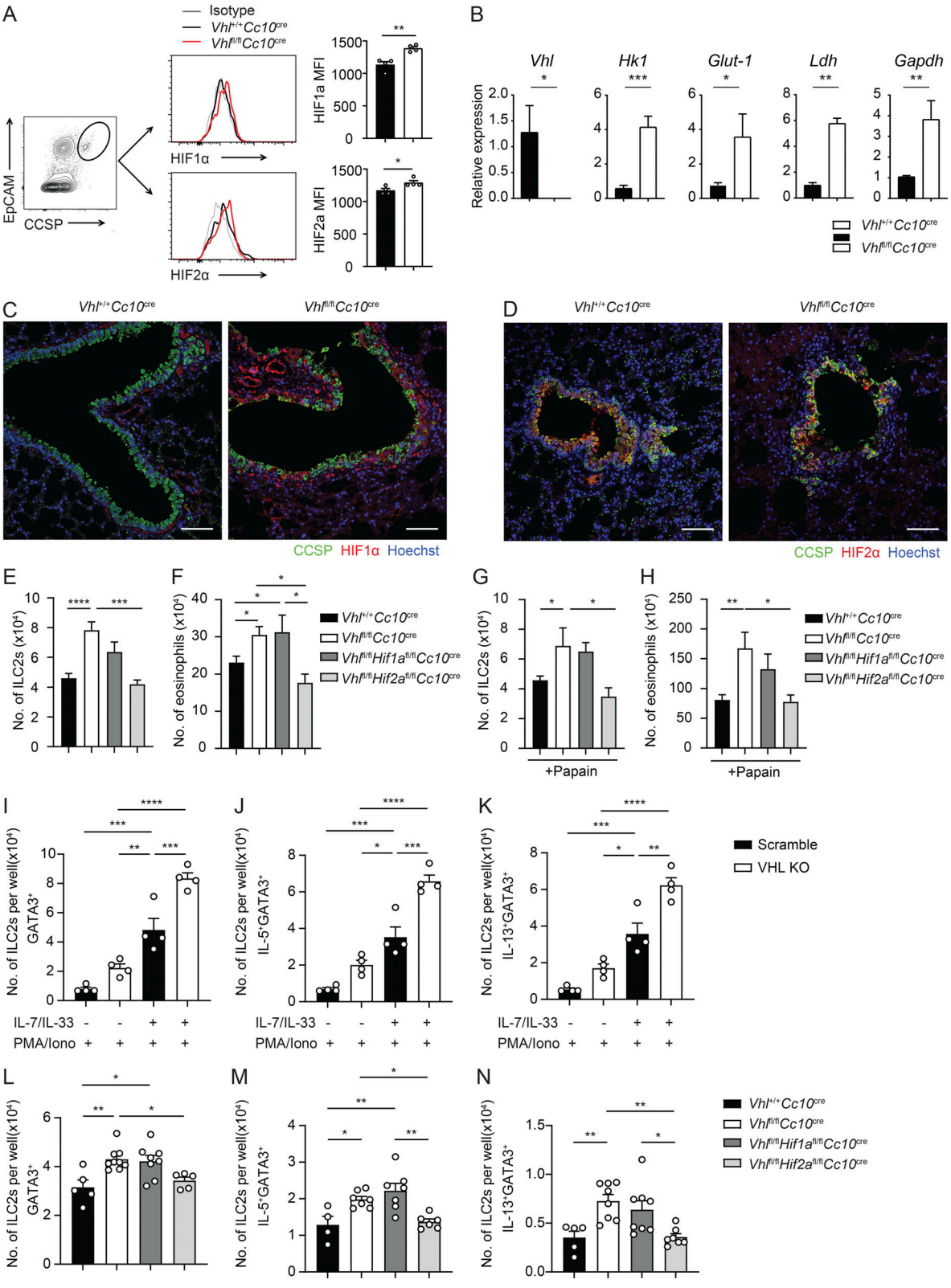

Figure 4. **HIF2α deletion reverses the enhanced ILC2 activity in VHL deficiency. (A)** Representative data show HIF1α and HIF2α expression in bronchiolar epithelial cells from WT and cKO mice. Mean fluorescence intensity (MFI) was measured by flow cytometry. **(B)** Gene expression of glycolytic enzymes increased by VHL deficiency. qPCR analysis was performed to determine mRNA levels of the indicated genes. **(A and B)** *, P < 0.05; **, P < 0.01; ***, P < 0.001 (Student's *t* test). **(C and D)** Representative sections of the lung from WT and cKO mice stained for CCSP (green), HIF1α (red), and Hoechst (blue; C); CCSP (green), HIF2α (red), and Hoechst (blue; D); 20× magnification; scale bar, 50 µm. **(E and F)** Total numbers of ILC2s (E) and eosinophils (F) in lung tissue from mice with indicated genotypes. **(G and H)** Mice with indicated genotypes were analyzed upon papain administration. The number of ILC2s (G) and eosinophils

(H) were assessed by flow cytometric analysis. **(E–H)** *n* = 3–5 mice/group, pooled from at least three independent experiments. **(I–K)** Lung bronchiolar club cell–like C22 cells with CRISPR-mediated deletion of Vhl were cocultured with ILC2s for 3 d with or without IL-7 (10 ng/ml) and IL-33 (10 ng/ml); Scramble-gRNA–transfected cell (Scramble, black) and VHL KO cell (VHL KO, white). The numbers of GATA3$^+$ total ILC2s (I) and IL-5– or IL-13–secreting ILC2s (J and K) were counted after 2.5-h stimulation with PMA and ionomycin. *n* = 4 sets of cells/group. Data are representative of two independent experiments. **(L–N)** Conditioned culture medium containing concentrated BAL fluid from WT (black), VHL cKO (white), VHL/HIF1α DKO (dark gray), and VHL/HIF2α DKO (light gray) were plated with cultured ILC2s for 3 d in the presence of IL-7 (10 ng/ml). The numbers of GATA3$^+$ total ILC2s were determined (L), and the absolute numbers of ILC2s expressing IL-5 (M) and IL-13 (N) were counted. For flow cytometry, cells were activated with PMA and ionomycin for 2.5 h before intracellular staining of indicated cytokines. *n* = 2–3 mice/group pooled from at least two independent experiments. **(E–N)** *, P < 0.05; **, P < 0.01; ***, P < 0.001; ****, P < 0.0001 by one-way ANOVA followed by Tukey's test. All data presented as mean ± SEM.

These data indicate that soluble factors induced by the VHL–HIF2α pathway in epithelia could directly contribute to ILC2 growth and activation.

ADM mediates VHL–HIF2α signaling in VHL-deleted mice

To identify factors involved in communication with ILC2, we performed bulk RNA-seq and compared the transcriptomes of sorted bronchiolar epithelial cells from WT and VHL cKO treated with PBS or papain. We selected CD45$^-$CD31$^-$EpCAM$^+$ lung epithelial cells, and further selected cells deficient for both MHCII and podoplanin (PDPN). This yielded a population of bronchiolar epithelial cells that highly expressed club cell markers *Ccsp* and *Cyp2f2*, but not *Sftpc*, a marker for type II alveolar epithelial cells (AECs; Fig. S4, A and B). Transcriptional profiles from VHL-deficient bronchiolar epithelial cells were distinguished from WT controls by principal component analysis (PCA), particularly with regard to PC1, under both PBS- and papain-treated conditions (Fig. 5 A). We then used gene set enrichment analysis (GSEA) to investigate genes differentially expressed between WT and VHL cKO mice. As expected, gene expression signatures corresponding to hypoxia and glycolysis were positively enriched, and gene sets related to oxidative phosphorylation and fatty acid metabolism were negatively enriched in VHL-deficient mice compared with WT controls (Figs. 5, B and C; and S4, C and D).

The bronchiolar epithelia expressed minimal *Il25* (not depicted), but detectable *Il33* and *Tslp* from either WT or cKO mice. The quantity of *Il33* mRNA and protein, however, was not changed between bronchiolar epithelial cells from cKO and WT mice at steady state (Fig. 5, D and E). Similar results were obtained at steady state for TSLP (Fig. 5, F and G), or after papain treatment for both cytokines' mRNA (Fig. S4 E). We further analyzed expression of IL-33 and TSLP proteins in the airway epithelia using immunofluorescence. We determined that surfactant protein C (SP-C)$^+$ type II AECs were the major source of IL-33, rather than CCSP$^+$ bronchiolar epithelial club cells (Fig. 5 E). In contrast, both bronchiolar club cells and type II AECs expressed TSLP (Fig. 5 G). Importantly, we found that the amount of TSLP in bronchiolar club cells was comparable between WT and VHL cKO mice (Fig. 5 G).

Recently, diverse types of molecules including cytokines, growth factors, neuropeptides, lipid mediators, and cell–cell signaling molecules were found to modulate ILC2 effector functions (Hurrell et al., 2018; Klose and Artis, 2016). We investigated which of those molecules were expressed by bronchiolar epithelial cells and whether VHL deficiency influenced their expression by analyzing whole-transcriptome sequences from lung epithelial cells from WT and VHL cKO mice under resting and papain-stimulated conditions. As shown in Fig. 5 H, mRNA expression encoding several ILC2 regulatory proteins was comparable between WT and VHL cKO mice under resting as well as papain-treated conditions. However, mRNA expression of genes encoding complement factor C3 and growth factor VEGFα, known to affect ILC2 (Gour et al., 2018; Lee et al., 2004), were significantly increased in resting epithelial cells from cKO mice (Fig. 5, H and I), although this difference did not reach statistical significance compared with cells from papain-treated mice. As shown in Fig. S4 F, VEGFα protein was increased at steady state in VHL cKO mice, confirming the RNA-seq data. Because club cell VHL deficiency did not alter epithelium-derived alarmin expression, and because VEGFα and C3 were not significantly increased following papain treatment, we considered it unlikely that VEGFα and C3 could explain all of the effects on ILC2.

To specify molecular mediators involved in activating ILC2s in VHL cKO mice, we performed transcriptome analysis of sort-purified bronchiolar epithelial cells and visualized gene overlaps with Venn diagrams. We found that 670 genes were upregulated from epithelial cells of VHL cKO mice compared with WT mice treated with PBS, while the expression of 241 genes was augmented in cells from papain-treated VHL cKO mice in comparison to WT controls (Fig. 6 A). 88 genes were increased in VHL-deficient epithelial cells under both conditions. Among these differentially expressed genes, only 14 encoded extracellular regions or secreted soluble proteins. We also identified 41 genes that were downregulated in VHL cKO epithelial cells under both resting and papain-stimulated conditions, of which only 5 encoded soluble factors (Fig. 6 A).

Volcano plots of RNA-seq datasets of cKO versus WT samples revealed genes that were significantly down- or upregulated under a resting state (Fig. 6 B). Of 14 upregulated genes encoding secreted proteins in cKO mice, *Adm*, which encodes the hormone peptide ADM, was identified as a potential candidate (Fig. 6 B). This conclusion was supported by its potential cellular function and the expression of mRNA encoding ADM receptors, especially *Calcr1*, *Ramp2*, and *Ramp3*, by lung ILC2s (Fig. 6 C), as revealed by reanalysis of previously published RNA-seq data (Ricardo-Gonzalez et al., 2018). Indeed, a heatmap showed that *Adm* was one of the most differentially expressed hypoxia-related genes (Fig. 6 D). We then analyzed *Adm* expression patterns in WT and VHL cKO lung epithelia based on RNA-seq at the resting state and following papain treatment. The data revealed that *Adm* expression was strongly induced under both conditions by VHL deficiency (Fig. 6 E). In addition, we observed

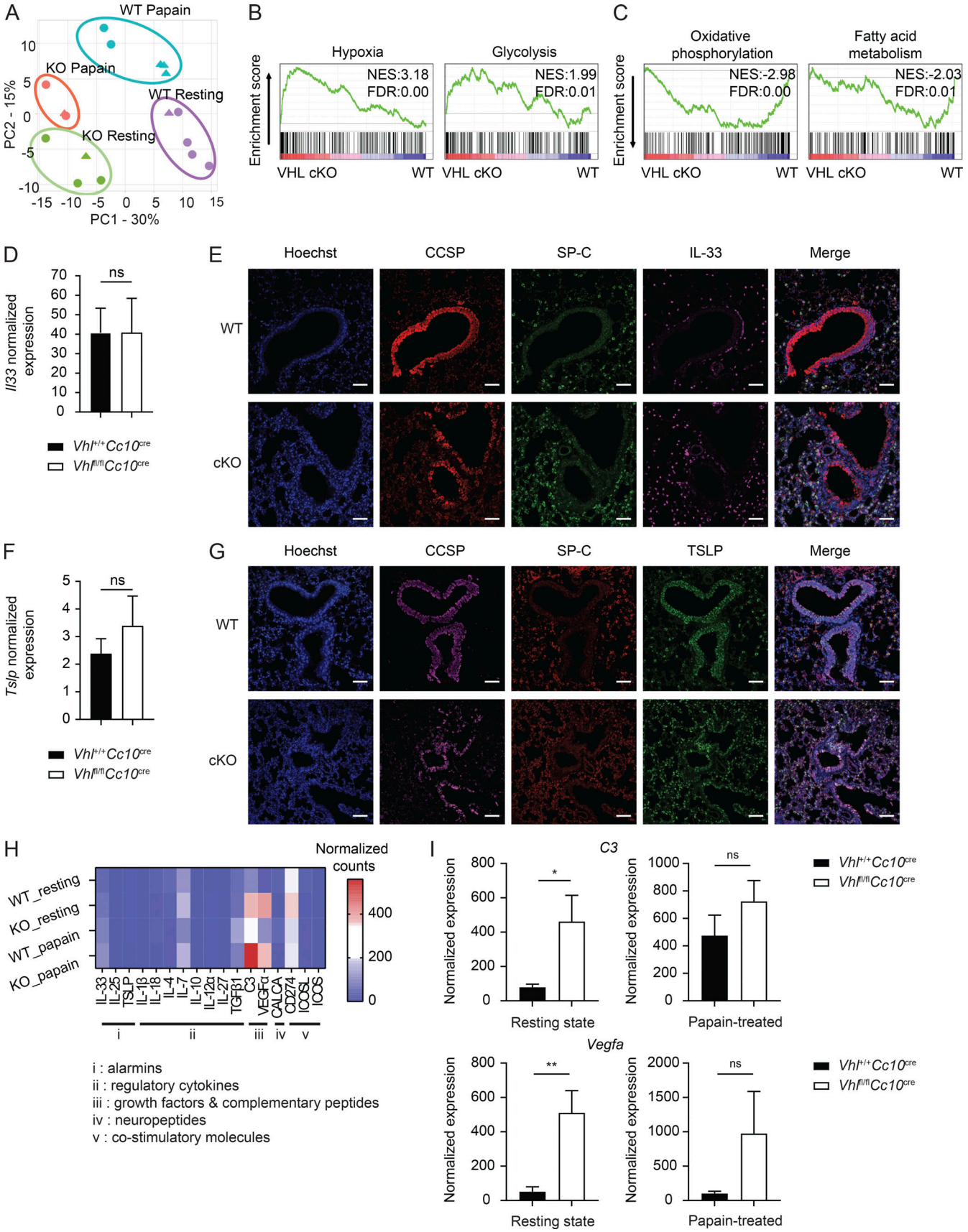

Figure 5. **VHL deficiency did not alter epithelium-derived alarmin expression. (A)** Bulk RNA sequencing of sorted bronchiolar epithelial cells of the indicated genotype and condition. Each symbol represents data from one sample pooled from three male (circle) or female (triangle) mice. PCA plot

representing each experimental group. **(B and C)** GSEA plots of hallmark gene set categories including hypoxia, glycolysis, oxidative phosphorylation, and fatty acid metabolism in VHL cKO versus WT bronchiolar epithelial cells at steady state. FDR, false discovery rate; NES, normalized enrichment score. **(D)** Expression of *Il33* in sorted lung bronchiolar epithelial cells from WT or cKO mice at steady state as determined by RNA-seq. **(E)** Representative section of the lungs from WT and cKO mice stained for CCSP (red), SP-C (green), IL-33 (magenta), and Hoechst (blue); 20× magnification; scale bar, 50 µm. Data are representative of two independent experiments (n = 3 mice/group). **(F)** Expression of *Tslp* in lung bronchiolar epithelial cells as in D. **(G)** Expression of TSLP protein (green) as in E. **(H)** Differential gene expression of selected genes that regulate ILC2 in lung epithelial cells from control and VHL cKO mice challenged with PBS or papain as measured by RNA-seq. **(I)** Normalized expression of *C3* and *Vegfa* gene in bronchiolar epithelial cells sorted from indicated mice. n = 3–5 samples/group for RNA-seq. Each sample pooled from three mice. *, P < 0.05; **, P < 0.01 (Student's t test). All data presented as mean ± SEM.

increased ADM in BAL fluid from VHL-deficient mice compared with WT mice under both PBS- and papain-treated conditions (Fig 6 F). Immunofluorescence imaging analysis showed that VHL-deficient bronchiolar epithelia expressed ADM at steady state, whereas WT mice did not (Fig. 6 G). We further examined the expression of ADM on WT mice after bleomycin instillation, and the data showed that bleomycin induced hypoxia (red) in the bronchiolar epithelial regions (gray) that express CCSP, and some of the CCSP$^+$ bronchiolar epithelial club cells express ADM (green; Fig. S5 A). Furthermore, VHL and HIF2α double knockout significantly ablated the stimulatory effect of VHL deficiency on lung epithelial cell–derived ADM production, but VHL and HIF1α DKO did not (Fig. 6 H).

To further understand the mechanisms by which HIF2α regulates ADM expression, we examined whether the *Adm* gene could serve as a direct target of HIF2α in bronchiolar epithelial cells. Analysis of the *Adm* gene revealed that there are several putative HRE regions in this genetic locus (Fig. 6 I). A chromatin immunoprecipitation (ChIP) assay was performed to determine whether HIF2α interacts with those putative binding sites. Notably, we found that HIF2α associated with all of the identified sites. Importantly, the HIF2α binding sites were correlated with histone H3 (trimethyl K4) modification in VHL KO cell lines compared with controls, suggesting an active transcription of the *Adm* gene due to VHL deficiency (Fig. 6 J).

We additionally examined the human bronchiolar epithelial cell line BEAS-2B to identify whether hypoxia could increase ADM synthesis in human lung epithelial cells. Hypoxia was induced by $CoCl_2$ or dimethyloxalylglycine (DMOG) treatment (Fig. 6 K), and consequently ADM was increased in BEAS-2B (Fig. 6, L and M). Overall, these data indicated that ADM expression was induced in VHL-deficient lung epithelia in an HIF2α-dependent manner.

ADM acts as an important regulator of ILC2 activation

To identify a role for bronchiolar epithelium-derived ADM in regulating ILC2s, we cultured freshly isolated ILC2s from bone marrow in the presence of ADM alone or in combination with IL-33. Addition of ADM to ILC2 cultures resulted in strong induction of IL-5 production and a percentage of IL-5–positive ILC2s comparable to IL-33–treated samples. In addition, ADM synergized with IL-33 to promote IL-5 production by ILC2s, whereas unlike IL-33 alone, treatment with ADM alone had no effect on IL-13 production by ILC2s (Fig. 7, A and B).

We examined whether ADM had functioned to increase and activate ILC2 cells in vivo. When mice were given ADM by the intranasal route for three consecutive days, this resulted in the development of airway inflammation accompanied by enhanced eosinophilia in lung tissues, compared with PBS-treated control mice (Fig. 7, C and D). The absolute numbers of ILC2s and KLRG1$^+$ activated ILC2s were increased in ADM-treated mice (Fig. 7 E). Further flow cytometric analysis revealed higher expression of ILC2 surface activation markers, including Sca-1 and KLRG1, in ADM-treated mice (Fig. 7 F).

To identify whether ADM had potential effector function in vivo in activating ILC2s during helminth infection, we infected mice with *N.b.* larvae with or without recombinant ADM administration (Fig. 7 G). As shown in Fig. 7 H, we observed a significant increase in the number of lung ILC2s and KLRG1-expressing activated ILC2s in ADM-administered mice 2 d after infection with *N.b.* ADM-treated mice also showed a trend of increased eosinophilic inflammation in comparison with PBS-treated mice after *N.b.* infection (Fig. S5 B). Further flow cytometric analysis revealed that ILC2s from ADM-treated mice expressed KLRG1 at a higher level on their surface and showed increased IL-5 production (Fig. S5,C and D). In addition, intestinal worm burden was significantly lower on day 7 after infection in ADM-treated mice compared with untreated mice, suggesting that ADM played an important role in worm expulsion (Fig. 7 I).

We added an ADM antagonist to cultures of ILC2 in BAL fluid obtained from either WT or VHL cKO mice. The antagonist, $ADM_{22–52}$, is an N-terminal truncated peptide that retains binding affinity for the ADM receptors without inducing a downstream cAMP response (Eguchi et al., 1994). We observed that the increased number and enhanced IL-5 production by ILC2s cultured with VHL-cKO conditioned medium was reversed when the ILC2s were cultured with VHL-cKO conditioned medium containing $ADM_{22–52}$ (Fig. 7 J). The antagonist had a mild effect on ILC2 IL-13 that was not statistically significant. These data indicate that soluble ADM from VHL-deficient epithelia contributed to ILC2 expansion and activation, which was abrogated by treatment with an ADM antagonistic peptide. In addition, in vivo administration of ADM antagonistic peptides abolished not only activation of ILC2s but also eosinophilia during papain-induced lung inflammation (Fig. 7, K–M). Taken together, these results demonstrated a crucial role for ADM in the regulation of pulmonary type 2 responses by regulating ILC2s.

Discussion

In this study, we demonstrated that increased hypoxia drives ILC2 activity and type 2 immune responses in the lung. We demonstrated this by selective deletion of genes in the VHL–HIF system in a subset of bronchiolar epithelial cells. We observed

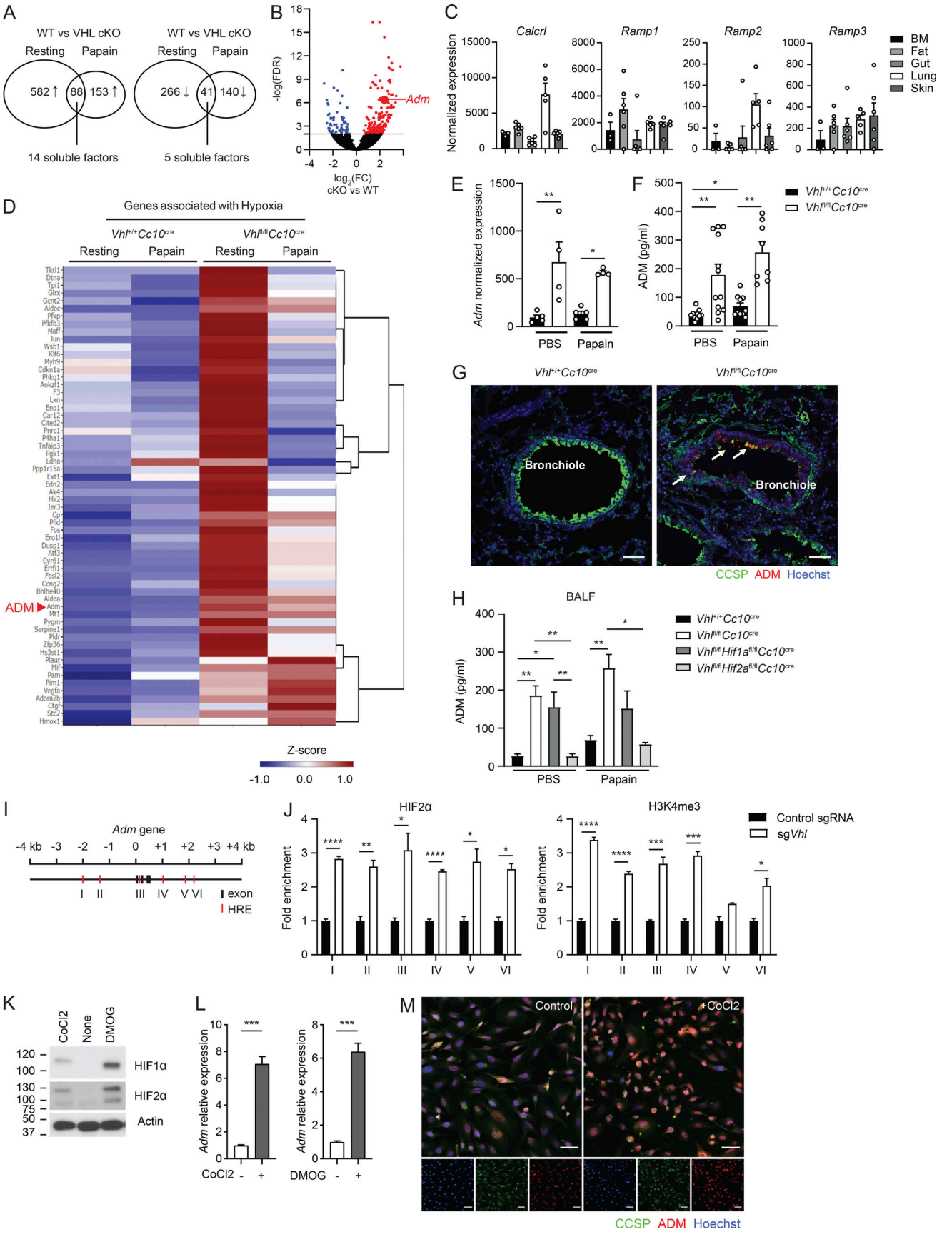

Figure 6. **ADM expression is regulated by VHL–HIF2α axis. (A)** Venn diagrams show the number of genes that were up- or downregulated in VHL cKO compared with WT epithelia under resting state and papain-induced inflammation. **(B)** Volcano plot of differential gene expression between bronchiolar

epithelial cells from WT and cKO mice at steady state. FC, fold-change; FDR, false discovery rate. **(C)** Analysis of published RNA-seq data for ADM receptor expression in ILC2s from indicated tissues. BM, bone marrow. **(D)** Heat maps of the indicated gene expression Z-scores of bronchiolar epithelial cells from resting state or papain-treated WT or cKO mice as measured by RNA-seq. Each column represents the average of one group of samples. **(E)** Normalized expression of *Adm* in bronchiolar epithelial cells sorted from indicated mice. *n* = 3–5 samples/group for RNA-seq; each sample pooled from three mice. **(F)** Concentrations of ADM in the BAL fluid. **(G)** Representative section of the lung from WT and cKO mice stained for CCSP (green), ADM (red), and Hoechst (blue); 20× magnification; scale bar, 50 µm. Arrows point to ADM-positive cells. Data are representative of two independent experiments. **(H)** Concentrations of ADM in the BAL fluid from WT, VHL cKO, VHL/HIF1α DKO, and VHL/HIF2α DKO mice. *n* = 2–7 mice/group, pooled from more than two independent experiments. **(E, F, and H)** *, P < 0.05; **, P < 0.01 by one-way ANOVA followed by Tukey's test. **(I)** Structural schematic of the mouse *Adm* gene with putative HREs. Black boxes for exon and red boxes for HRE are shown. **(J)** Binding of HIF2α and H3K4me3 on the *Adm* gene in control or VHL KO C22 cell line. Relative binding activity was normalized to binding in control cells. *n* = 3 sets/group. Data are representative of two independent experiments. **(K)** Cells were treated with $CoCl_2$ or DMOG, and lysates were immunoblotted to analyze hypoxia induction in BEAS-2B cells. **(L)** The expression of *Adm* was determined qPCR. **(M)** Representative images of control and $CoCl_2$-treated BEAS-2B cells stained for CCSP (green), ADM (red), and Hoechst (blue); 20× magnification; scale bars, 50 µm. **(J and L)** Data pooled from two or more independent experiments; bar graphs show mean ± SEM. *, P < 0.05; **, P < 0.01; ***, P < 0.001; ****, P < 0.0001 (Student's *t* test). Source data are available for this figure: SourceData F6.

this effect on ILC2 functions at resting state, and under both allergic or inflammatory conditions. We further identified epithelial cell–derived ADM as a critical mediator of the epithelium–ILC2 interaction in this VHL-controlled pathway; ADM expression was increased by stabilization of HIF2α in VHL-deficient club cells. At the molecular level, we showed that HIF2α directly bound to the HRE sites in the *Adm* gene. In addition, we showed that ADM promoted some of the effector function of ILC2s in vitro and in vivo. Our study thus revealed the crucial role of the VHL–HIF2α pathway, via the regulation of ADM expression in lung epithelia, in the control of ILC2 number and function and in the modulation of pulmonary allergic responses and the response to infections.

Airway epithelium carries out protective functions against constantly inhaled irritants that can damage lung tissue by secreting glycoaminoglycans and other substances. The epithelium also initiates pulmonary immune responses by producing cytokines and alarmins that are protective, but that also can impair normal lung physiological functions. ILC2s serve as the earliest effector cells responding to lung epithelial stimulation, and they play a critical role in orchestrating type 2 immunity and promoting tissue repair (Klose and Artis, 2016). Emerging findings suggest that multiple factors from various structural cells can enhance or repress ILC2 proliferation and effector functions in allergic inflammation (Hurrell et al., 2018; Klose and Artis, 2016). Here we have shown how the lung epithelia, especially CC10-expressing bronchiolar club cells, alert the immune system in response to oxygen-sensing by regulating ILC2 cells and type 2 immunity. Interestingly, we demonstrated that the epithelium–ILC2 cross talk induced by hypoxia was not via the production of well-characterized classic alarmins, such as TSLP, IL-25, and IL-33, by epithelial cells. Instead, we identified the peptide hormone ADM as the critical mediator for ILC2 population expansion, and IL-5, although IL-13 synthesis was not increased. Therefore, additional factors may be elicited from club cells exposed to hypoxic conditions to give the full activation of ILC2. Our data suggest that VEGFα and C3a are excellent candidate proteins for these additional signals, as transcripts for both were increased in the VHL cKO mice. Consistent with this hypothesis, increased lung inflammation and type 2 immunity were observed when club cells overexpressed VEGFα (Lee et al., 2004), but it was not determined whether ILC2s were responsible. Furthermore, it also was shown that ILC2 can respond to C3a, and that C3a is important for ILC2-mediated airway responses (Gour et al., 2018). Interestingly, VEGFα and C3a promoted increased IL-13 and some other cytokines, but relatively little IL-5, while ADM promoted IL-5 secretion. Therefore, it is possible that different tissue-derived signals activate ILC2s, leading to different aspects of type 2 immune responses.

Hypoxia has been linked to pulmonary diseases such as asthma, COPD, and pulmonary fibrosis, through stabilization of HIF transcription factors (Lee et al., 2019). Our study demonstrated that loss of VHL in club cells resulted in hypoxia and enhanced type 2 immunity via increased ILC2s, accompanied by abnormal and inflamed lungs with increased infiltrated immune cells and goblet cell hyperplasia. Our data do not rule out the possibility that cell types other than ILC2, including T cells, might respond to hypoxia in the lung to stimulate type 2 immunity. The response to hypoxia may be regulated differently, however, comparing the conducting and respiratory portions of the lung and considering different responding cell types. In fact, stabilization of HIF1α in alveolar type II epithelial cells, induced by acute lung injury, causes metabolic alteration that attenuated pulmonary chronic inflammation (Eckle et al., 2013). More recently, we demonstrated that HIF1α-driven glycolysis in alveolar macrophages ameliorated lung inflammation and fibrosis by inhibiting ILC2 activation (Zhang et al., 2018). How exactly each of the diverse cell types senses oxygen changes in the lung needs further investigation.

It is notable that the effects of hypoxia in club cells were largely reversed by HIF2α deletion. It has been reported that HIF isoforms, including HIF1α and HIF2α, exhibit different tissue- or cell type–restricted expression profiles, as well as different DNA binding selectivity. Although HIF1α is more widely expressed across tissues and cell types, HIF2α is preferentially expressed in normal tissues and selective cell types in the kidney, intestine, lung, and liver (Jain et al., 1998; Lee et al., 2019; Wiesener et al., 2003). Indeed, we observed that bronchiolar epithelium dominantly expressed HIF2α, which is present in resting normal lung epithelium and is further stabilized by VHL deficiency. A recent study classified populations of the mouse tracheal epithelium with cell type–specific markers by single-cell RNA-seq (Montoro et al., 2018). By reanalyzing these data, we found that $CCSP^+$ club cells and basal cells enriched in mouse upper airway epithelium specifically expressed HIF2α rather than HIF1α. Such cell type–specific expression profiles of HIF isoforms implied that

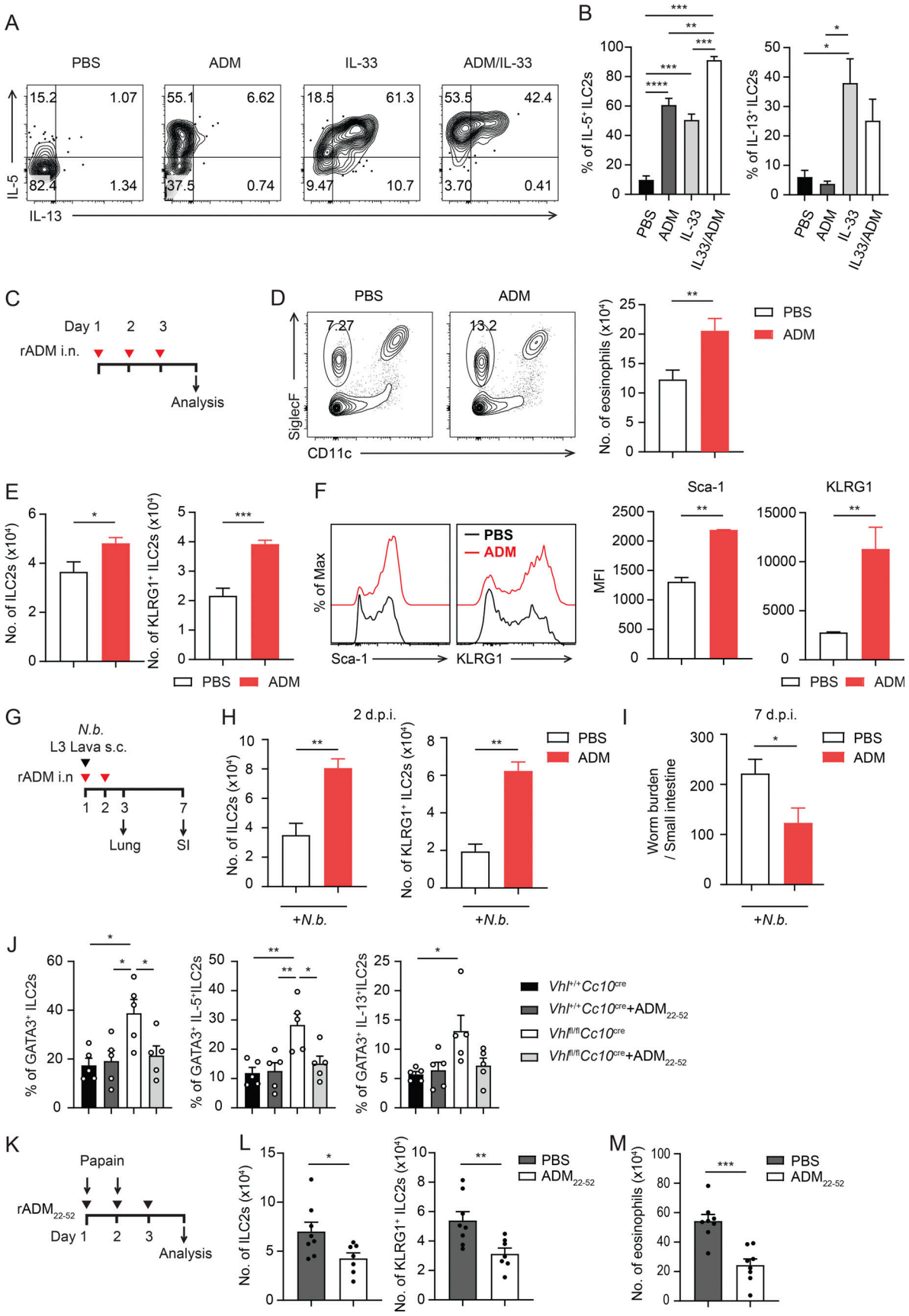

Figure 7. **ADM potentiates ILC2-mediated lung inflammation. (A)** Flow cytometric analysis of ILC2s stimulated in vitro with ADM, IL-33, or both in the presence of PMA and ionomycin for 2.5 h. **(B)** Percentage of IL-5+ and IL-13+ ILC2s as determined by intracellular cytokine staining. *n* = 3 sets/group. Data are

representative of two independent experiments. *, P < 0.05; **, P < 0.01; ***, P < 0.001; ****, P < 0.0001 by one-way ANOVA followed by Tukey's test. **(C)** Experimental protocol for intranasal treatment with ADM. **(D)** Flow cytometric analysis (left) and the number (right) of eosinophils. **(E)** Total number of lung ILC2s and KLRG1$^+$ ILC2s were assessed by flow cytometry. **(F)** Flow cytometric analysis of expression (left) and quantification of mean fluorescence intensity (MFI; right) of Sca-1 and KLRG1 in ILC2s. **(G)** Experimental protocol for *N.b.* infection treated with recombinant ADM. **(H)** Total numbers of ILC2s and KLRG1$^+$ ILC2s were assessed on day 2 after *N.b.* infection. **(I)** Worm burden in the small intestine 7 d after infection; n = 3–5 mice/group. **(D–I)** Data are representative of three independent experiments. *, P < 0.05; **, P < 0.01; ***, P < 0.001 (Student's t test). **(J)** The percentage of cytokine-positive ILC2s was quantified after in vitro culture with conditioned medium containing BAL fluid from WT and cKO mice in the absence or presence of ADM22-52. n = 2–3 mice/group pooled from two independent experiments. *, P < 0.05; **, P < 0.01 by one-way ANOVA followed by Tukey's test. **(K)** Experimental protocol for intranasal administration of ADM22-52 and/or papain. **(L and M)** Total number of lung ILC2s, KLRG1$^+$ ILC2s (L), and eosinophils (M) were assessed by flow cytometry. n = 3–4 mice/group pooled from two independent experiments; bar graphs show mean ± SEM; *, P < 0.05; **, P < 0.01; ***, P < 0.001 (Student's t test).

HIF2α conducts an important and unique role in bronchiolar epithelial cell function and downstream signaling that can affect the pulmonary microenvironment. Our findings are consistent with previous studies that showed that HIF2α in bronchiolar club cells induced the expression of the transcription factor FOXM1, which enabled epithelial proliferation and drove hyperproliferation of pulmonary neuroepithelial bodies in response to hypoxia (Hodson et al., 2016; Macias et al., 2018; Urrutia and Aragonés, 2018), as well as the expression of resistin-like α (RELMα), which causes pulmonary hypertension (Torres-Capelli et al., 2016).

We demonstrated that *Adm* gene expression was regulated by HIF2α in VHL-deficient bronchiolar epithelial cells, and ADM controls ILC2 expansion and activation. ADM is a multifunctional peptide that is expressed by epithelial cells of various tissues, especially in the lung (Martinez et al., 1995), and may be involved in the pathogenesis of chronic inflammatory lung diseases such as COPD and asthma (Ceyhan et al., 2001; Mandal et al., 2015; Mandal et al., 2019). Consistent with this hypothesis, serum levels of ADM were positively correlated with the clinical score of patients with COPD (Dres et al., 2017; Mandal et al., 2015; Mandal et al., 2019; Meng et al., 2014; Schuetz et al., 2015). Our RNA-seq data suggested that *Adm* transcription was increased in VHL-deficient epithelial cells under homeostatic and papain-induced inflammatory conditions. Consistently, ADM concentrations in the BAL fluid in VHL-deficient lung were significantly higher than in controls. Importantly, increased *Adm* expression due to VHL deficiency was reverted by genetic ablation of *Hif2a*. Inspection revealed that there were several putative HRE regions in the mouse *Adm* gene, and our ChIP data suggested they served as HIF2α direct binding sites to promote gene expression.

ADM is a member of the calcitonin gene-related peptide (CGRP) family, along with CGRP, intermedin, and amylin, which are structurally related peptides (Poyner et al., 2002). CGRP mediates its effects via a heterodimeric receptor composed of RAMP1 and calcitonin-like receptor, whereas the ADM receptor consists of calcitonin-like receptor with either a RAMP2 or RAMP3 subunit forming the heterodimer (Poyner et al., 2002). Communication between epithelial cells and ILC2s via ADM is further supported by expression of transcripts encoding each of the subunits of the ADM receptor by ILC2 cells from bone marrow and peripheral tissues (Ricardo-Gonzalez et al., 2018). Importantly, ADM activated ILC2 effector functions both in vitro and in vivo. We also observed that the enhanced activity of ILC2s due to VHL deficiency was reversed by treatment with the ADM antagonistic peptide $ADM_{22–52}$. Hence, our results revealed that ADM mediates communication between lung epithelium and ILC2s to drive type 2 inflammation in the airways.

In sum, our study highlights that hypoxia regulation of the VHL–HIF2α axis is required for epithelium-ILC2 communication through ADM expression by bronchiolar epithelial cells. Therefore, our data provide a new pathway whereby the mucosal barrier regulates type 2 immune responses initiated by ILC2. Our study highlights that regulation of the VHL–HIF2α–ADM axis may represent a therapeutic target in the treatment and prevention of allergic lung diseases.

Materials and methods

Mice

Mice used in this study were on a C57BL/6 background. $Vhl^{fl/fl}$, $Hif1a^{fl/fl}$, and $Hif2a^{fl/fl}$ mice were purchased from Jackson Laboratory. Cc10-Cre mice (Simon et al., 2006) were generously provided by T. Mariani (Harvard Medical School, Boston, MA) and used to cross with $Vhl^{fl/fl}$, $Hif1a^{fl/fl}$, and $Hif2a^{fl/f}$ mice. All lines were backcrossed to C57BL/6 strains for at least eight generations. Animals were cohoused after weaning, and littermate controls were used in all experiments. Male and female mice were sex matched and used at 8–12 wk of age, unless otherwise indicated. Mice were age-matched within each experiment, but pooled results include both male and female mice. All animals were maintained in the animal facility under an animal protocol approved by the Institutional Animal Care and Use Committee at La Jolla Institute for Immunology.

Models of lung inflammation

For papain-induced type 2 inflammation in the lung, mice were anesthetized with isoflurane, and then 25 µg of papain or PBS in a total volume of 40 µl was given i.n. on days 1, 2, and 3. BAL fluid and lungs were harvested and analyzed on day 4. For animal model of recombinant ADM treatment, mice were anesthetized with isoflurane, and 25 µg of recombinant ADM (Anaspec), or 100 µg of $ADM_{22–52}$ (Anaspec) in a total volume of 40 µl was administered i.n. at indicated time points. Inflammatory cells in the lung were assessed on day 4. For helminth infection, third-stage larvae (L3) of *N.b.*, which was obtained from Dr. D. Artis (Weill Cornell Medicine, New York, NY), were purified with a Baermann technique (Camberis et al., 2003). After washing three times in PBS, live worms were counted. On day 0, 300 or 500 purified worms were injected subcutaneously in 250 µl PBS. Mice were euthanized at the indicated time points

to collect tissues for analysis or to count worm burden. For induction of bleomycin-induced pulmonary inflammation, mice were anesthetized with isoflurane and treated with 0.1 U bleomycin (Sigma-Aldrich) or PBS in a volume of 40 µl intratracheally, followed by analysis on day 7 to assess pulmonary inflammation.

Immunoblot

In some experiments, animals were i.n. injected with 60 mg/kg of Hypoxyprobe (Hypoxyprobe Inc.) to detect tissue hypoxia. After 2 h, mice were sacrificed, and lungs were collected. The lung of each mouse was homogenized and lysed with radioimmunoprecipitation assay buffer (1% Triton X-100, 280 mM NaCl, 0.1% SDS, 0.2% sodium deoxycholate, 5 mM EGTA, and proteinase inhibitor). Immunoblotting was performed with the following antibodies: anti-HIF1α (Cayman Chemical), anti–β-actin (Santa Cruz), and anti-hypoxyprobe mAb (Hypoxyprobe Inc.).

Cell isolation from mouse tissues

Cells from BAL fluids were collected by flushing the lung three times with 1 ml of cold PBS containing 0.2% BSA through the trachea. Collected BAL fluids were centrifuged at 500 *g* for 3 min. For isolation of lung tissue cells, the lungs were minced and digested with 0.1 mg/ml type VIII collagenase (Sigma-Aldrich) and 25 µg/ml DNase I (Worthington) for 1.5 h at 37°C on a rotator. To isolate leukocytes from the lungs, digested tissues were filtered through 70-µm cell strainers. Red blood cells were lysed with ACK buffer.

Lung histopathology

Lungs were harvested, fixed in zinc formalin (Medical Chemical Corp.), and embedded in paraffin for sectioning (4 µm). H&E-, PAS-, and Masson's trichrome–stained slides were converted to whole slide images (Zeiss Axio Scan) and evaluated and scored by a board-certified pathologist for airway inflammation and other pathological changes. The total histologic score is the sum of the score for each criterion including thrombosis, alveolar hemorrhage, necrosis, hemosiderophages, interstitial pneumonia/pneumonitis, hyperemia, bronchial endothelial cell hypoplasia, emphysema, pulmonary edema, perivascular inflammation, and iBALT hyperplasia in the lung.

Flow cytometry and cell sorting

Dead cells were routinely excluded with Zombie Aqua or Yellow Fixable Viability Kit (BioLegend). Single-cell suspensions were kept at 4°C and incubated on ice with the following conjugated antibodies in PBS. For ILC2 staining, lineage-positive cells were excluded by staining for CD3ε (145-2C11), CD4 (clone GK1.5), CD8α (clone 53-6.7), CD11c (N418), CD11b (M1/70), CD19 (6D5), TCRβ (H57-597), TCRγδ (GL3), NK1.1 (PK136), Gr1 (RB6-8C5), Ter119 (TER-119), and B220 (RA3-6B2), and then cells were stained with the following antibodies for surface staining; Thy1.2 (53-2.1), CD25 (PC61.5), CD127 (A7R34), Sca-1 (D7), T1/ST2 (DJ8), KLRG1 (2F1), MHCII (M5/114.15.2), PD-1 (29F.1A12), and ICOS (15F9). Eosinophils were identified as $CD45^+CD11C^{-/lo}SiglecF^+$.

Lung cells were used for isolation of $CD45^-CD31^-EpCAM^+MHCII^-CD49f^+CD103^+$ bronchiolar epithelial cells. For isolation of bone marrow ILC2s, lineage-negative cells were first enriched by using mouse Lineage Cell Depletion Kit (Miltenyi Biotec) following the manufacturer's instructions. Then, $Lin^-CD25^+CD127^+T1ST2^+$ cells were further sorted on FACS Aria (BD Biosciences).

Intracellular staining

For intracellular staining of transcription factors, cells were stained with antibodies to surface antigens, fixed, permeabilized with Fixation/Permeabilization buffer (eBioscience) according to the manufacturer's instructions, and further stained with antibodies specific for GATA3 (FJK-16s), T-bet (4B10), RORγt (B2D), HIF1α (241812; R&D Systems), and HIF2α (ep190b; Novus). For intracellular staining for cytokines, cells were stimulated with PMA (10 ng/ml) and ionomycin (1 mM) in the presence of GolgiStop (BD Bioscience) for 4 h at 37°C. After surface marker staining, cells were fixed and permeabilized with Fixation/Permeabilization buffer and stained with anti-IFNγ (XMG1.2), anti–IL-4 (11B11), anti–IL-5 (TRFK5), anti–IL-13 (eBio13A), and anti–IL-17 (TC11-18H10.1) antibodies. All antibodies used in flow cytometry were purchased from eBioscience, BioLegend, or BD Biosciences unless otherwise indicated. Flow cytometry analysis was performed on an LSRII instrument (BD Biosciences) or Fortessa flow cytometer (BD Biosciences), and data were analyzed using FlowJo software (TreeStar) and compiled using Prism 8 (GraphPad Software).

Real-time PCR analysis

Total RNA was extracted with TRIzol (Invitrogen), and cDNA was synthesized with an iScript cDNA Synthesis Kit (Bio-Rad). qPCR reactions were performed using iTaq Universal SYBR Green Supermix (Bio-Rad) with CFX384 real-time system (Bio-Rad). The level of mRNA was normalized to the housekeeping gene β-actin or cyclophilin-A. The primer sequences used in this study are listed in Table S1.

C22 cell culture and *Vhl* CRISPR lentiviral transduction of C22 cells

The C22 (ECACC 07021401) cells were maintained in DMEM containing 4% FBS, 100 U/ml penicillin, 1% streptomycin, 0.25 µg/ml endothelin-1, 10 µg/ml insulin, 5 µg/ml transferrin, 7.5 µg/ml endothelial cell growth supplement, 0.025 µg/ml epidermal growth factor, 0.36 µg/ml hydrocortisone, and 0.02 µg/ml T3 (Demello et al., 2002). Cells were incubated in 10% CO_2 at 33°C under proliferative conditions in the presence of IFNγ. sgRNA-containing oligonucleotides were cloned into the pXPR_001 lenti CRISPR vector containing a mAmetrine reporter gene. The following primers were used: sgVhl-F, 5′-CACCGACAA AGGCAGCACGACGCGC′-3′; and sgVhl-R, 5′-AAAC GCGCGTCGT GCTGCCTTTGTC′-3′. Lentiviruses containing sgRNAs were packaged in 293T cells by using TransIT-LT1 transfection reagent (Mirus) following the manufacturer's instructions. The supernatant containing sgRNA-expressing lentivirus was collected 48 h after transfection and used for transducing C22 cell lines in C22 complete medium. To maximize sgRNA expression, mAmetrine-positive cells were sorted, and the analysis for gene expression was performed 3 d after transfection.

In vitro ILC2 culture

$Lin^-CD25^+CD127^+ST2^+$ ILC2s were sorted from Lin^- enriched bone marrow cells by flow cytometry on FACS Aria (BD Biosciences). The cells were cultured and expanded in MEM-α complete medium containing 20% FBS, 1% penicillin-streptomycin, 10 ng/ml IL-7 (Peprotech), and 10 ng/ml IL-33 (R&D Systems). ILC2s were seeded onto the C22-bronchiolar club cell–like cell line monolayers or cultured with BAL fluid conditioned from mouse BAL fluid of indicated genotype, at a density of 3,000–10,000 ILC2s per well. BAL fluid was collected by flushing the lung with 1 ml of cold PBS through the trachea; cells in the BAL fluid were depleted by centrifugation at 500 *g* for 5 min, and BAL fluid was concentrated and supplemented in MEM-α ILC2 culture medium for making conditioned medium. After 3 d of culture, following stimulation with PMA (10 ng/ml) and ionomycin (1 mM), cells were stained for analysis of intracellular expression of IL-5, IL-13, and IL-4. Bone marrow ILC2s were sorted and plated at a density of 5,000–10,000 cells per well with or without 10 ng/ml of IL-33 and 1 µM of recombinant ADM or $ADM_{22–52}$ for 4 h in the presence of PMA (10 ng/ml) and ionomycin (1 mM). Treated ILC2s were analyzed on Fortessa flow cytometer (BD Biosciences).

Immunofluorescence

For lung cell staining, lung tissues were flushed and fixed with zinc formalin (Medical Chemical Corp.) overnight and embedded in paraffin for sectioning (4 µm). Immunofluorescent staining was performed, followed by antigen retrieval with sodium citrate buffer (10 mM sodium citrate and 0.05% Tween 20, pH 6.0). Tissue sections were treated with 10% normal donkey serum (Jackson ImmunoResearch) and stained with the following antibodies in antibody dilution buffer supplemented with 0.3% Triton X-100 (Sigma-Aldrich) and 1% BSA: anti–hypoxiprobe-1 Mab (Hypoxyprobe Inc.), anti-CCSP (Upstate), anti–SP-C (Upstate), anti–IL-33 (R&D Systems), anti-TLSP biotinylated (R&D Systems), anti-HIF1α (Novus), anti-HIF2α (Novus), and anti-ADM (Biorbyt). Secondary antibodies were purchased from Invitrogen. Samples were mounted with Prolong Gold (Thermo Fisher Scientific), and images of representative tissues were captured by LSM 780 confocal microscope and analyzed with Zen software (Carl Zeiss).

RNA-seq

Mouse bronchiolar epithelial cells were isolated and sorted using a FACS Aria and pooled from three mice per sample. RNA extraction was performed using RNeasy mini kit (Qiagen). RNA-seq libraries were prepared using the SMARTer Stranded Total RNA-seq Kit v2 (TaKaRa; Picelli et al., 2014). Libraries were sequenced using Illumina HiSeq 2500 to generate 50-bp single-end reads performed by LJI Sequencing Core Facility. Three to five biological replicates were generated.

RNA-seq analysis

The paired-end reads that passed Illumina filters were filtered for reads aligning to tRNA, rRNA, adapter sequences, and spike-in controls. The reads were then aligned to GRCm38.p4 reference genome using TopHat (v 1.4.1). Read counts to each genomic feature were obtained with the htseq-count program (v 0.7.1) using the "union" option. After removing absent features, the raw counts were then imported to R/Bioconductor package DESeq2 (v1.6.3) to identify differentially expressed genes among samples. P values for differential expression were calculated using the Wald test for differences between the base means of two conditions. These P values were then adjusted for multiple test correction using Benjamini–Hochberg algorithm. We considered genes differentially expressed between two groups of samples when the DESeq2 analysis resulted in an adjusted P value of <0.10 and the difference in gene expression was 1.5-fold. Principal component analysis was performed using function prcomp in R v3.6.1. PCA plots were created with principal components 1 and 2 as the x and y axis, respectively, using ggplot2. GSEA was performed using the GseaPreranked method with classic scoring scheme. The sequences used in this article have been submitted to GEO under accession number GSE197007.

Rank files for each DE comparison of interest were generated by assigning a rank of $-\log_{10}$ (P value) to genes with $\log_2$ fold-change greater than zero and a rank of $\log_{10}$(P value) to genes with $\log_2$ fold-change less than zero. Row-scaled heatmap of TPM values were created with heatmaply in *R*. Venn diagrams were generated using *R* function venn.diagram.

ADM ELISA

BAL fluid from each mouse was collected, frozen, and stored at −80°C until processed. The concentration of ADM was quantified by using Mouse Adrenomedullin/ADM ELISA Kit (Novus) according to the manufacturer's instruction.

ChIP

For each sample, cells were fixed with 1% formaldehyde for 5 min at RT, lysed in lysis buffer, and sonicated by using E220 Focused-ultrasonicator (Covaris). Sheared DNA-protein was immunoprecipitated with 2.5 µg anti-HIF2α antibodies (ep190b; Novus), anti-H3K4me3 (Abcam), or isotype control IgG overnight with rotation at 4°C. Immunoprecipitated samples were reverse-crosslinked, and DNA was eluted. qPCR was performed and analyzed. Primers for qPCR are listed in Table S2.

In vitro cell culture and hypoxia induction

Human bronchiolar epithelial cells (BEAS-2B cell line; American Type Culture Collection) were treated with 100 µM DMOG or 400 µM $CoCl_2$ for 24 h in RPMI 1640 containing 10% FBS. ADM was visualized using anti-ADM antibodies (Biorbyt) by LSM 780 confocal microscope and analyzed with Zen software (Carl Zeiss).

Statistical analysis

Statistical significance was assessed by unpaired two-tailed Student's *t* test or one-way ANOVA with post hoc Tukey's multiple comparison test with Prism v8 (GraphPad Software; detailed in figure legends).

Online supplemental material

Fig. S1 shows that hypoxia occurs in the lung following either inflammation or *N.b.* infection and that deletion of *Vhl* in club

cells of the lung epithelium, which increases hypoxia, at steady state causes activation of ILC2 but few changes in $CD4^+$ T cells. Fig. S2 shows that in mice with deletion of *Vhl* in club cells, bleomycin treatment increases ILC2 and type 2 immune responses. Fig. S3 shows that deletion of *Vhl* in a cell line representing club cells leads to increased expression of hypoxia-related genes. Fig. S4 shows RNA-seq results from preparations enriched for club cells from *Vhl*-deleted and control mice showing predicted increases in glycolysis genes. Fig. S5 shows that bleomycin treatment or *N.b.* infection leads to secretion of ADM, which activates ILC2. Table S1 lists primers used for qPCR. Table S2 provides primers used for the ChIP assay.

Acknowledgments

We thank Dr. T. Mariani for providing CC10-cre mice and Dr. D. Artis for providing *N.b.* We thank the staff of the Flow Cytometry Core (supported by National Institutes of Health grant S10RR027366), Sequencing Core, Bioinformatics Core, Microscopy & Histology Core, and the Department of Laboratory Animal Care (DLAC) at La Jolla Institute for Immunology for technical assistance, and A. Sethi for bioinformatic analysis.

This work is supported by National Institutes of Health grants R01AI123398 and U01 AI125955.

Author contributions: J. Han and Y.-C. Liu conceived the project. J. Han conducted key experiments and performed data analysis. Q. Wan assisted with in vitro experiments, and G.-Y. Seo and J.H. Lee, with infection experiments. K. Kim provided advice on histology and provided histology analysis. S. el Baghdady performed mouse breeding. M. Kronenberg supervised the study and designed experiments. J. Han wrote the manuscript, and M. Kronenberg and Y.-C. Liu edited the manuscript.

The authors declare no competing financial interests.

Submitted: 21 September 2021
Revised: 21 February 2022
Accepted: 4 April 2022

References

Artis, D., and H. Spits. 2015. The biology of innate lymphoid cells. *Nature*. 517: 293–301. https://doi.org/10.1038/nature14189

Camberis, M., G. Le Gros, and J. Urban Jr. 2003. Animal model of *Nippostrongylus brasiliensis* and *Heligmosomoides polygyrus*. *Curr. Protoc. Immunol.* Chapter 19:Unit 19.12. https://doi.org/10.1002/0471142735.im1912s55

Ceyhan, B.B., S. Karakurt, and N. Hekim. 2001. Plasma adrenomedullin levels in asthmatic patients. *J. Asthma*. 38:221–227. https://doi.org/10.1081/jas-100000109

Darby, I.A., and T.D. Hewitson. 2016. Hypoxia in tissue repair and fibrosis. *Cell Tissue Res.* 365:553–562. https://doi.org/10.1007/s00441-016-2461-3

Demello, D.E., S. Mahmoud, J. Ryerse, and J.W. Hoffmann. 2002. Generation and characterization of a conditionally immortalized lung clara cell line from the H-2Kb-tsA58 transgenic mouse. *In Vitro Cell. Dev. Biol. Anim.* 38:154–164. https://doi.org/10.1290/1071-2690(2002)038<0154:GACOAC>2.0.CO;2

Dres, M., P. Hausfater, F. Foissac, M. Bernard, L.M. Joly, M. Sebbane, A.L. Philippon, C. Gil-Jardine, J. Schmidt, M. Maignan, et al. 2017. Mid-regional pro-adrenomedullin and copeptin to predict short-term prognosis of COPD exacerbations: A multicenter prospective blinded study. *Int. J. Chron. Obstruct. Pulmon. Dis.* 12:1047–1056. https://doi.org/10.2147/COPD.S126400

Eckle, T., K. Brodsky, M. Bonney, T. Packard, J. Han, C.H. Borchers, T.J. Mariani, D.J. Kominsky, M. Mittelbronn, and H.K. Eltzschig. 2013. HIF1A reduces acute lung injury by optimizing carbohydrate metabolism in the alveolar epithelium. *PLOS Biol.* 11:e1001665. https://doi.org/10.1371/journal.pbio.1001665

Eguchi, S., Y. Hirata, H. Iwasaki, K. Sato, T.X. Watanabe, T. Inui, K. Nakajima, S. Sakakibara, and F. Marumo. 1994. Structure-activity relationship of adrenomedullin, a novel vasodilatory peptide, in cultured rat vascular smooth muscle cells. *Endocrinology*. 135:2454–2458. https://doi.org/10.1210/endo.135.6.7988431

Goodwin, J., H. Choi, M.H. Hsieh, M.L. Neugent, J.M. Ahn, H.N. Hayenga, P.K. Singh, D.B. Shackelford, I.K. Lee, V. Shulaev, et al. 2018. Targeting hypoxia-inducible factor-1α/pyruvate dehydrogenase kinase 1 axis by dichloroacetate suppresses bleomycin-induced pulmonary fibrosis. *Am. J. Respir. Cell Mol. Biol.* 58:216–231. https://doi.org/10.1165/rcmb.2016-0186OC

Gour, N., U. Smole, H.-M. Yong, I.P. Lewkowich, N. Yao, A. Singh, E. Gabrielson, M. Wills-Karp, and S. Lajoie. 2018. C3a is required for ILC2 function in allergic airway inflammation. *Mucosal Immunol.* 11: 1653–1662. https://doi.org/10.1038/s41385-018-0064-x

Halim, T.Y.F., R.H. Krauss, A.C. Sun, and F. Takei. 2012. Lung natural helper cells are a critical source of Th_2 cell-type cytokines in protease allergen-induced airway inflammation. *Immunity*. 36:451–463. https://doi.org/10.1016/j.immuni.2011.12.020

Hammad, H., and B.N. Lambrecht. 2015. Barrier epithelial cells and the control of type 2 immunity. *Immunity*. 43:29–40. https://doi.org/10.1016/j.immuni.2015.07.007

Higgins, D.F., K. Kimura, W.M. Bernhardt, N. Shrimanker, Y. Akai, B. Hohenstein, Y. Saito, R.S. Johnson, M. Kretzler, C.D. Cohen, et al. 2007. Hypoxia promotes fibrogenesis in vivo via HIF-1 stimulation of epithelial-to-mesenchymal transition. *J. Clin. Invest.* 117:3810–3820. https://doi.org/10.1172/JCI30487

Hodson, E.J., L.G. Nicholls, P.J. Turner, R. Llyr, J.W. Fielding, G. Douglas, I. Ratnayaka, P.A. Robbins, C.W. Pugh, K.J. Buckler, et al. 2016. Regulation of ventilatory sensitivity and carotid body proliferation in hypoxia by the PHD_2/HIF-2 pathway. *J. Physiol.* 594:1179–1195. https://doi.org/10.1113/JP271050

Huang, Y., L. Guo, J. Qiu, X. Chen, J. Hu-Li, U. Siebenlist, P.R. Williamson, J.F. Urban, and W.E. Paul. 2015. IL-25-responsive, lineage-negative KLRG1hi cells are multipotential "inflammatory" type 2 innate lymphoid cells. *Nat. Immunol.* 16:161–169. https://doi.org/10.1038/ni.3078

Hurrell, B.P., P. Shafiei Jahani, and O. Akbari. 2018. Social networking of group two innate lymphoid cells in allergy and asthma. *Front. Immunol.* 9:2694. https://doi.org/10.3389/fimmu.2018.02694

Jain, S., E. Maltepe, M.M. Lu, C. Simon, and C.A. Bradfield. 1998. Expression of ARNT, $ARNT_2$, HIF_1 alpha, HIF_2 alpha and Ah receptor mRNAs in the developing mouse. *Mech. Dev.* 73:117–123. https://doi.org/10.1016/s0925-4773(98)00038-0

Klose, C.S.N., and D. Artis. 2016. Innate lymphoid cells as regulators of immunity, inflammation and tissue homeostasis. *Nat. Immunol.* 17: 765–774. https://doi.org/10.1038/ni.3489

Lee, C.G., H. Link, P. Baluk, R.J. Homer, S. Chapoval, V. Bhandari, M.J. Kang, L. Cohn, Y.K. Kim, D.M. McDonald, and J.A. Elias. 2004. Vascular endothelial growth factor (VEGF) induces remodeling and enhances TH_2-mediated sensitization and inflammation in the lung. *Nat. Med.* 10: 1095–1103. https://doi.org/10.1038/nm1105

Lee, J.W., J. Ko, C. Ju, and H.K. Eltzschig. 2019. Hypoxia signaling in human diseases and therapeutic targets. *Exp. Mol. Med.* 51:1–13. https://doi.org/10.1038/s12276-019-0235-1

Macias, D., A.S. Cowburn, H. Torres-Torrelo, P. Ortega-Sáenz, J. López-Barneo, and R.S. Johnson. 2018. HIF-2α is essential for carotid body development and function. *eLife*. 7:e34681.

Mandal, J., M. Roth, L. Bubendorf, S. Savic, M. Tamm, and D. Stolz. 2015. Disease specific effects of adrenomedullin in COPD and asthma derived human bronchial epithelial cells. *Eur. Respir. J.* 46:PA5103. https://doi.org/10.1183/13993003.congress-2015.pa5103

Mandal, J., M. Roth, E. Papakonstantinou, L. Fang, S. Savic, M. Tamm, and D. Stolz. 2019. Adrenomedullin mediates pro-angiogenic and pro-inflammatory cytokines in asthma and COPD. *Pulm. Pharmacol. Ther.* 56:8–14. https://doi.org/10.1016/j.pupt.2019.01.006

Martinez, A., M.J. Miller, E.J. Unsworth, J.M. Siegfried, and F. Cuttitta. 1995. Expression of adrenomedullin in normal human lung and in pulmonary

tumors. *Endocrinology*. 136:4099–4105. https://doi.org/10.1210/endo.136.9.7649118

Meng, D.-Q., X.-J. Li, X.-Y. Song, J.-B. Xin, and W.-B. Yang. 2014. Diagnostic and prognostic value of plasma adrenomedullin in COPD exacerbation. *Respir. Care*. 59:1542–1549. https://doi.org/10.4187/respcare.03046

Montoro, D.T., A.L. Haber, M. Biton, V. Vinarsky, B. Lin, S.E. Birket, F. Yuan, S. Chen, H.M. Leung, J. Villoria, et al. 2018. A revised airway epithelial hierarchy includes CFTR-expressing ionocytes. *Nature*. 560:319–324. https://doi.org/10.1038/s41586-018-0393-7

Palm, N.W., R.K. Rosenstein, and R. Medzhitov. 2012. Allergic host defences. *Nature*. 484:465–472. https://doi.org/10.1038/nature11047

Picelli, S., O.R. Faridani, A.K. Björklund, G. Winberg, S. Sagasser, and R. Sandberg. 2014. Full-length RNA-seq from single cells using Smart-seq2. *Nat. Protoc.* 9:171–181. https://doi.org/10.1038/nprot.2014.006

Poyner, D.R., P.M. Sexton, I. Marshall, D.M. Smith, R. Quirion, W. Born, R. Muff, J.A. Fischer, and S.M. Foord. 2002. International union of pharmacology. XXXII. The mammalian calcitonin gene-related peptides, adrenomedullin, amylin, and calcitonin receptors. *Pharmacol. Rev.* 54:233–246. https://doi.org/10.1124/pr.54.2.233

Price, A.E., H.E. Liang, B.M. Sullivan, R.L. Reinhardt, C.J. Eisley, D.J. Erle, and R.M. Locksley. 2010. Systemically dispersed innate IL-13-expressing cells in type 2 immunity. *Proc. Natl. Acad. Sci. USA*. 107:11489–11494. https://doi.org/10.1073/pnas.1003988107

Pulendran, B., and D. Artis. 2012. New paradigms in type 2 immunity. *Science*. 337:431–435. https://doi.org/10.1126/science.1221064

Rackley, C.R., and B.R. Stripp. 2012. Building and maintaining the epithelium of the lung. *J. Clin. Invest.* 122:2724–2730. https://doi.org/10.1172/JCI60519

Ricardo-Gonzalez, R.R., S.J. Van Dyken, C. Schneider, J. Lee, J.C. Nussbaum, H.-E. Liang, D. Vaka, W.L. Eckalbar, A.B. Molofsky, D.J. Erle, and R.M. Locksley. 2018. Tissue signals imprint ILC_2 identity with anticipatory function. *Nat. Immunol.* 19:1093–1099. https://doi.org/10.1038/s41590-018-0201-4

Roan, F., K. Obata-Ninomiya, and S.F. Ziegler. 2019. Epithelial cell-derived cytokines: More than just signaling the alarm. *J. Clin. Invest.* 129:1441–1451. https://doi.org/10.1172/JCI124606

Rokicki, W., M. Rokicki, J. Wojtacha, and A. Dżeljijli. 2016. The role and importance of club cells (Clara cells) in the pathogenesis of some respiratory diseases. *Kardiochir. Torakochirurgia Pol.* 13:26–30. https://doi.org/10.5114/kitp.2016.58961

Schofield, C.J., and P.J. Ratcliffe. 2004. Oxygen sensing by HIF hydroxylases. *Nat. Rev. Mol. Cell Biol.* 5:343–354. https://doi.org/10.1038/nrm1366

Schuetz, P., R. Marlowe, and B. Müller. 2015. The prognostic blood biomarker proadrenomedullin for outcome prediction in patients with chronic obstructive pulmonary disease (COPD): A qualitative clinical review. *Clin. Chem. Lab. Med.* 53:521–539. https://doi.org/10.1515/cclm-2014-0748

Simon, D.M., M.C. Arikan, S. Srisuma, S. Bhattacharya, L.W. Tsai, E.P. Ingenito, F. Gonzalez, S.D. Shapiro, and T.J. Mariani. 2006. Epithelial cell PPAR[gamma] contributes to normal lung maturation. *FASEB J.* 20:1507–1509. https://doi.org/10.1096/fj.05-5410fje

Torres-Capelli, M., G. Marsboom, Q.O.Y. Li, D. Tello, F.M. Rodriguez, T. Alonso, F. Sanchez-Madrid, F. García-Rio, J. Ancochea, and J. Aragonés. 2016. Role of Hif2α oxygen sensing pathway in bronchial epithelial club cell proliferation. *Sci. Rep.* 6:25357. https://doi.org/10.1038/srep25357

Tzouvelekis, A., V. Harokopos, T. Paparountas, N. Oikonomou, A. Chatziioannou, G. Vilaras, E. Tsiambas, A. Karameris, D. Bouros, and V. Aidinis. 2007. Comparative expression profiling in pulmonary fibrosis suggests a role of hypoxia-inducible factor-1alpha in disease pathogenesis. *Am. J. Respir. Crit. Care Med.* 176:1108–1119. https://doi.org/10.1164/rccm.200705-683OC

Urrutia, A.A., and J. Aragonés. 2018. HIF oxygen sensing pathways in lung biology. *Biomedicines*. 6:E68. https://doi.org/10.3390/biomedicines6020068

Whitsett, J.A., and T. Alenghat. 2015. Respiratory epithelial cells orchestrate pulmonary innate immunity. *Nat. Immunol.* 16:27–35. https://doi.org/10.1038/ni.3045

Wiesener, M.S., J.S. Jürgensen, C. Rosenberger, C.K. Scholze, J.H. Hörstrup, C. Warnecke, S. Mandriota, I. Bechmann, U.A. Frei, C.W. Pugh, et al. 2003. Widespread hypoxia-inducible expression of HIF-2alpha in distinct cell populations of different organs. *FASEB J.* 17:271–273. https://doi.org/10.1096/fj.02-0445fje

Zaiss, D.M.W., W.C. Gause, L.C. Osborne, and D. Artis. 2015. Emerging functions of amphiregulin in orchestrating immunity, inflammation, and tissue repair. *Immunity*. 42:216–226. https://doi.org/10.1016/j.immuni.2015.01.020

Zhang, W., Q. Li, D. Li, J. Li, D. Aki, and Y.-C. Liu. 2018. The E3 ligase VHL controls alveolar macrophage function via metabolic-epigenetic regulation. *J. Exp. Med.* 215:3180–3193. https://doi.org/10.1084/jem.20181211

Supplemental material

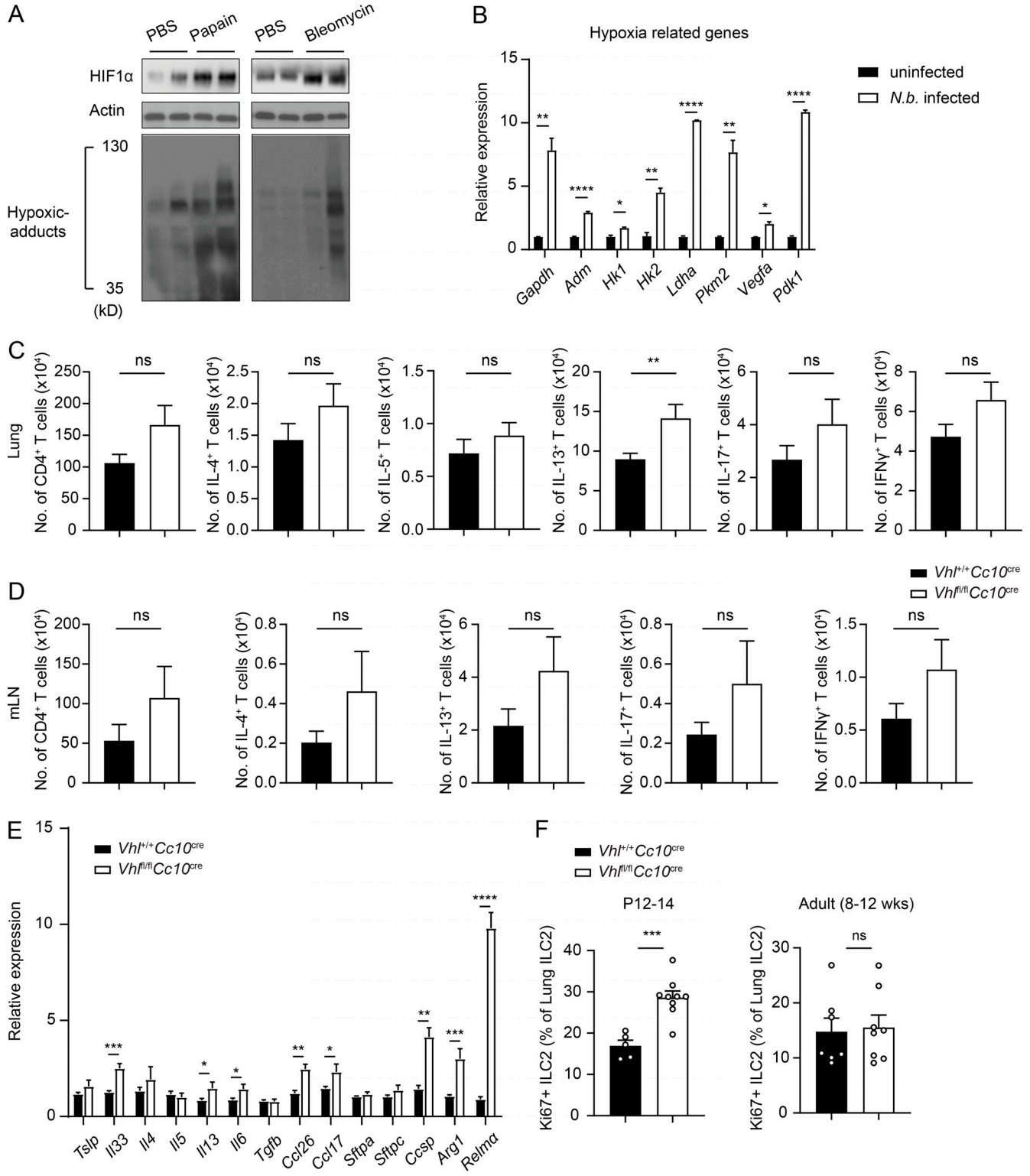

Figure S1. **Phenotypic analysis of VHL-deficient mice at resting state. (A)** Immunoblotting analysis of HIFα induction in whole-lung lysates from control and challenged mice. Each lane represents an individual animal. **(B)** Expression of hypoxia-related genes increased by *N.b.* infection in the lung. qPCR analysis was performed to determine mRNA levels of the indicated genes. *n* = 2–3 mice/group. Data are representative of two independent experiments. **(C and D)** CD4⁺ T cells in lung and mLN from WT and VHL cKO were assessed by flow cytometry. **(E)** Expression of type 2 related genes induced by VHL deficiency. RT-qPCR analysis was performed to determine mRNA levels of the indicated genes. Data are pooled from at least three independent experiments. *n* = 3–5 mice/group pooled from more than three independent experiments. **(F)** Percentage of Ki67⁺ ILC2s in the lung at the indicated age. **(B–F)** *n* = 2–5 mice/group pooled from two independent experiments. Error bars indicate SEM; *, P < 0.05; **, P < 0.01; ***, P < 0.001; ****, P < 0.0001 (Student's *t* test). Source data are available for this figure: SourceData FS1.

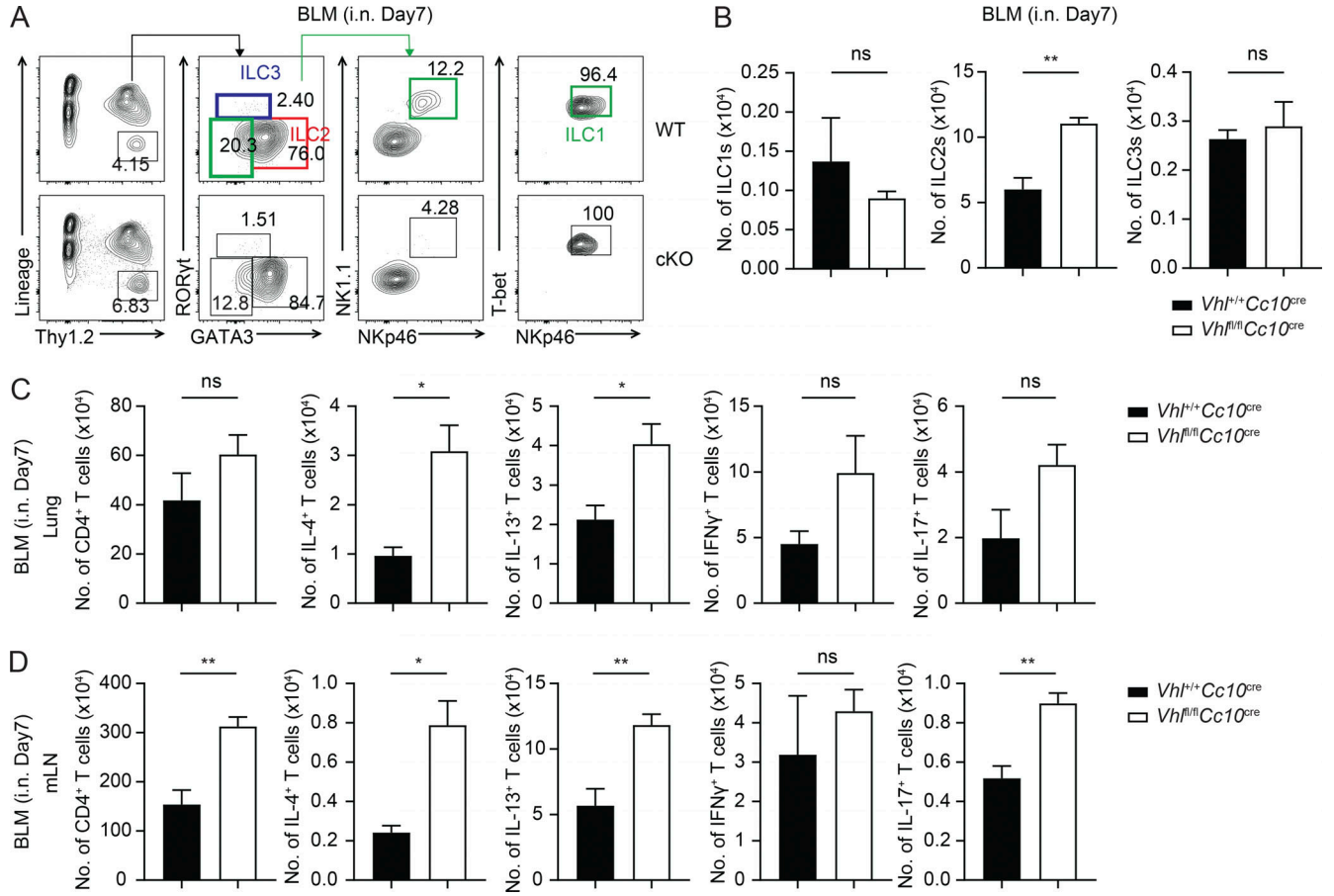

Figure S2. **VHL deficiency enhances ILC2-mediated type 2 immune response. (A and B)** Flow cytometric analysis of the lung ILC subtypes from WT and VHL cKO mice challenged with bleomycin. **(C and D)** Total number of cytokine-secreting CD4⁺ T cells in lung (C) and mLN (D) from WT and VHL cKO mice. **(B–D)** *n* = 3–5 mice/group pooled from three independent experiments. Error bars indicate SEM. *, P < 0.05; **, P < 0.01 (Student's *t* test).

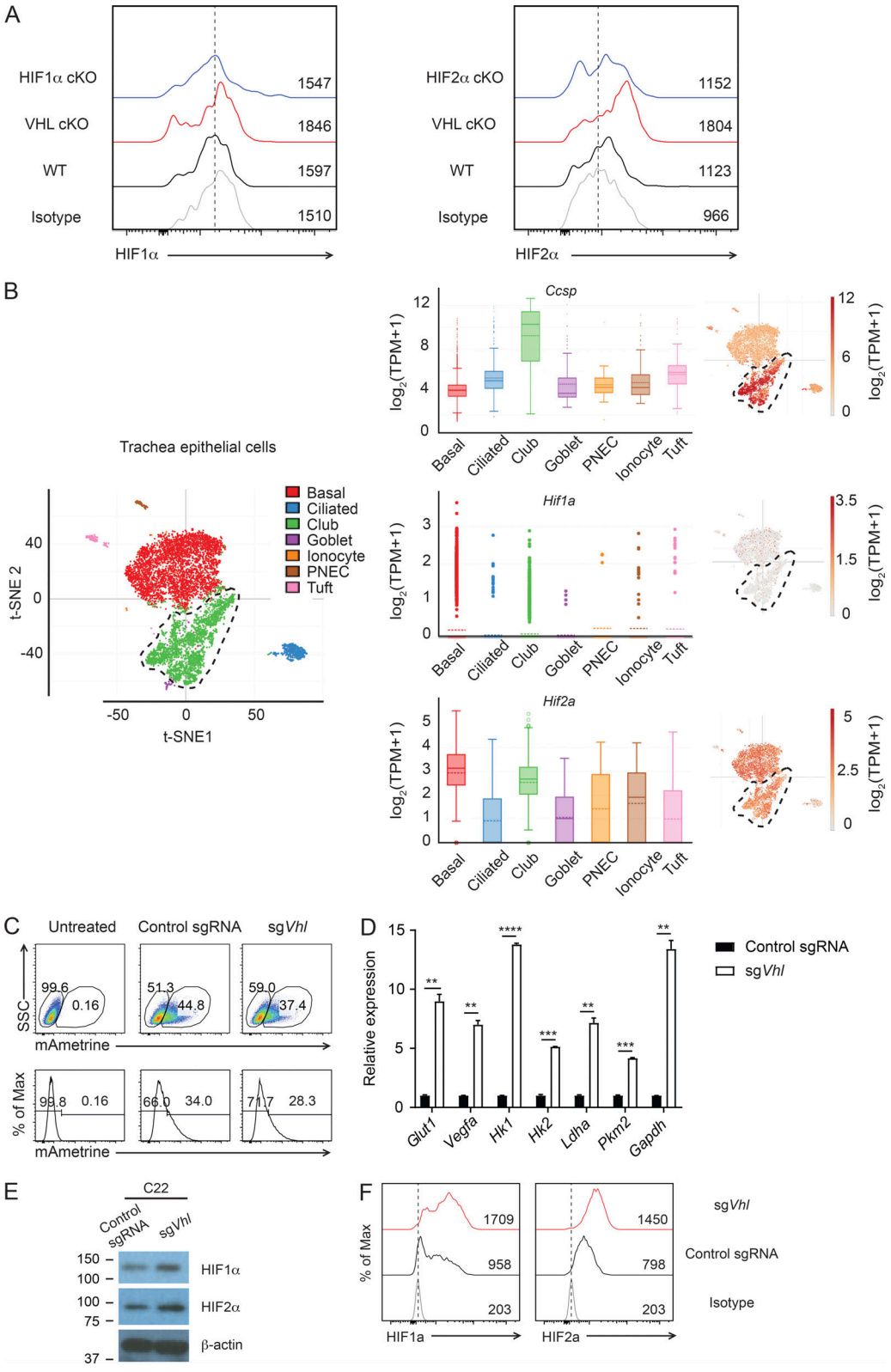

Figure S3. **HIF expression by lung epithelial cells and generation of VHL knockout cell line. (A)** Representative data shows HIF1α and HIF2α expression in bronchiolar epithelial cells of the indicated genotype. **(B)** Analysis of published (Montoro et al., 2018) single-cell RNA-seq transcriptional profiles of mouse tracheal epithelial cells. t-Distributed stochastic neighbor embedding (t-SNE) plots are colored by cluster assignment. Box plots show expression of *Ccsp*, *Hif1a*, and *Hif2a* in the indicated cell populations. **(C)** Flow cytometric analysis of transfection efficiency of C22 club cells. SSC, side scatter. **(D)** Gene expression of glycolytic enzymes by sorted VHL-deficient C22 cells and controls. Error bars indicate SEM; *, P < 0.05; **, P < 0.01; ***, P < 0.001; ****, P < 0.0001 (Student's *t* test). **(E)** Immunoblotting analysis of HIFα induction in VHL-deficient C22 cells and controls. **(F)** Flow cytometric analysis of expression of HIFα in control or VHL KO C22 cell line. Source data are available for this figure: SourceData FS3.

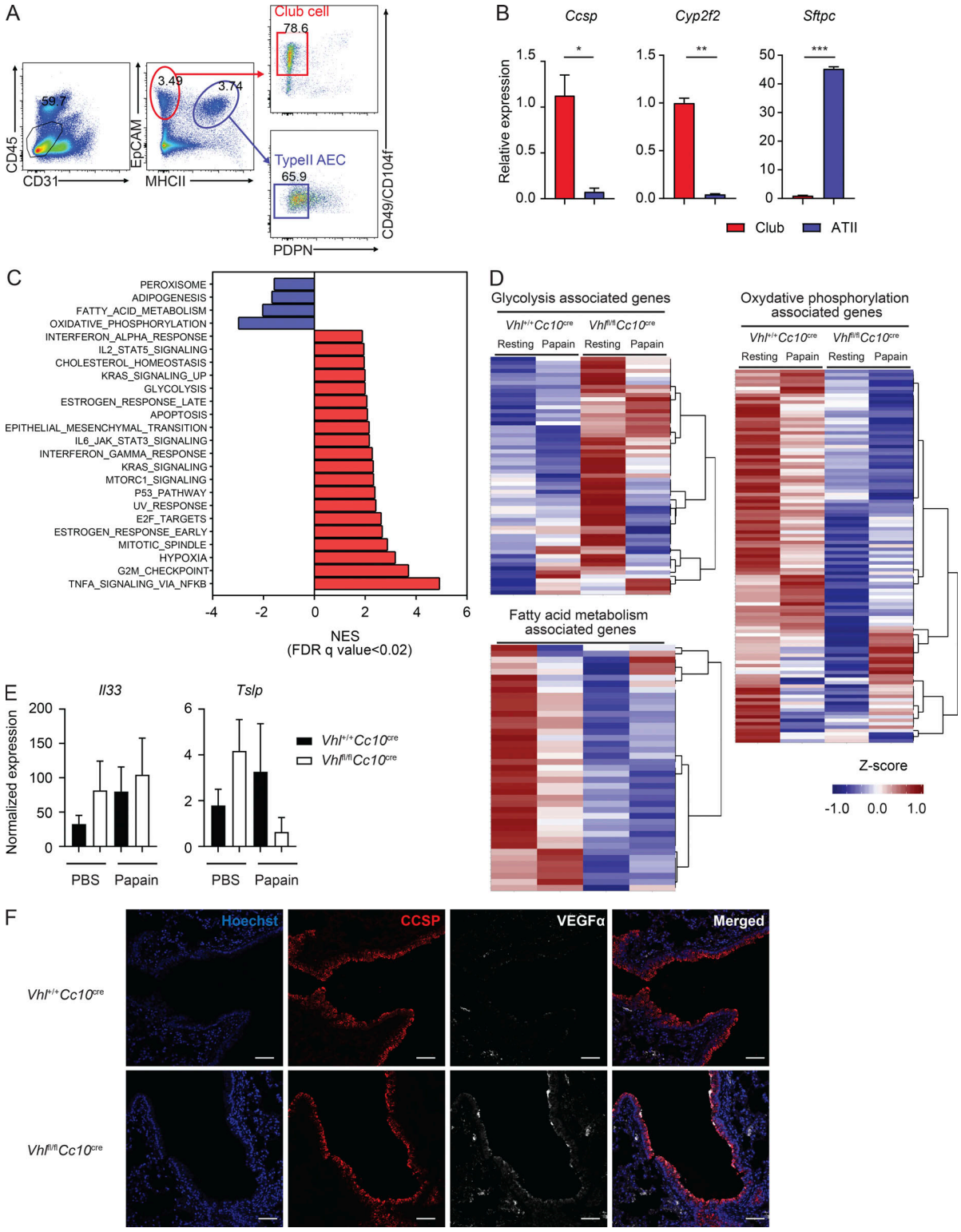

Figure S4. **Gating strategy for isolation of bronchiolar epithelial cells and bulk RNA-seq data analysis from WT and cKO mice. (A)** Gating strategy for lung bronchiolar epithelial cells. Gating was performed on live CD45⁻CD31⁻ cells and EpCAM⁺MHCII⁻PDPN⁻CD49/CD104f⁺ cells. **(B)** Expression of *Ccsp*, *Cyp2f2*, and *Sftpc* at resting state in the indicated epithelial cell populations determined by qPCR analysis. **(C)** Normalized enrichment scores (NESs) of GSEA hallmark gene sets of cKO versus WT epithelial cells under resting conditions. FDR, false discovery rate. **(D)** Heatmaps of the indicated gene expression Z-scores of bronchiolar epithelial cells from resting state or papain-treated WT or cKO mice as measured by RNA-seq. Each column represents the average of one group of samples. **(E)** Expression of *Il33* and *Tslp* in sorted lung bronchiolar epithelial cells from WT or cKO mice at steady state and after papain as determined by RNA-seq. *n* = 3–5 samples/group for RNA-seq. Each sample pooled from three mice. **(F)** Representative section of the lung from WT and cKO mice stained for CCSP (red), ADM (gray), and Hoechst (blue); 20× magnification; scale bars, 50 µm. Arrows point to ADM-positive cells. *n* = 2–3 mice/group. Data are representative of two independent experiments. Error bars indicate SEM. **(B)** *, P < 0.05; **, P < 0.01; ***, P < 0.001 (Student's *t* test).

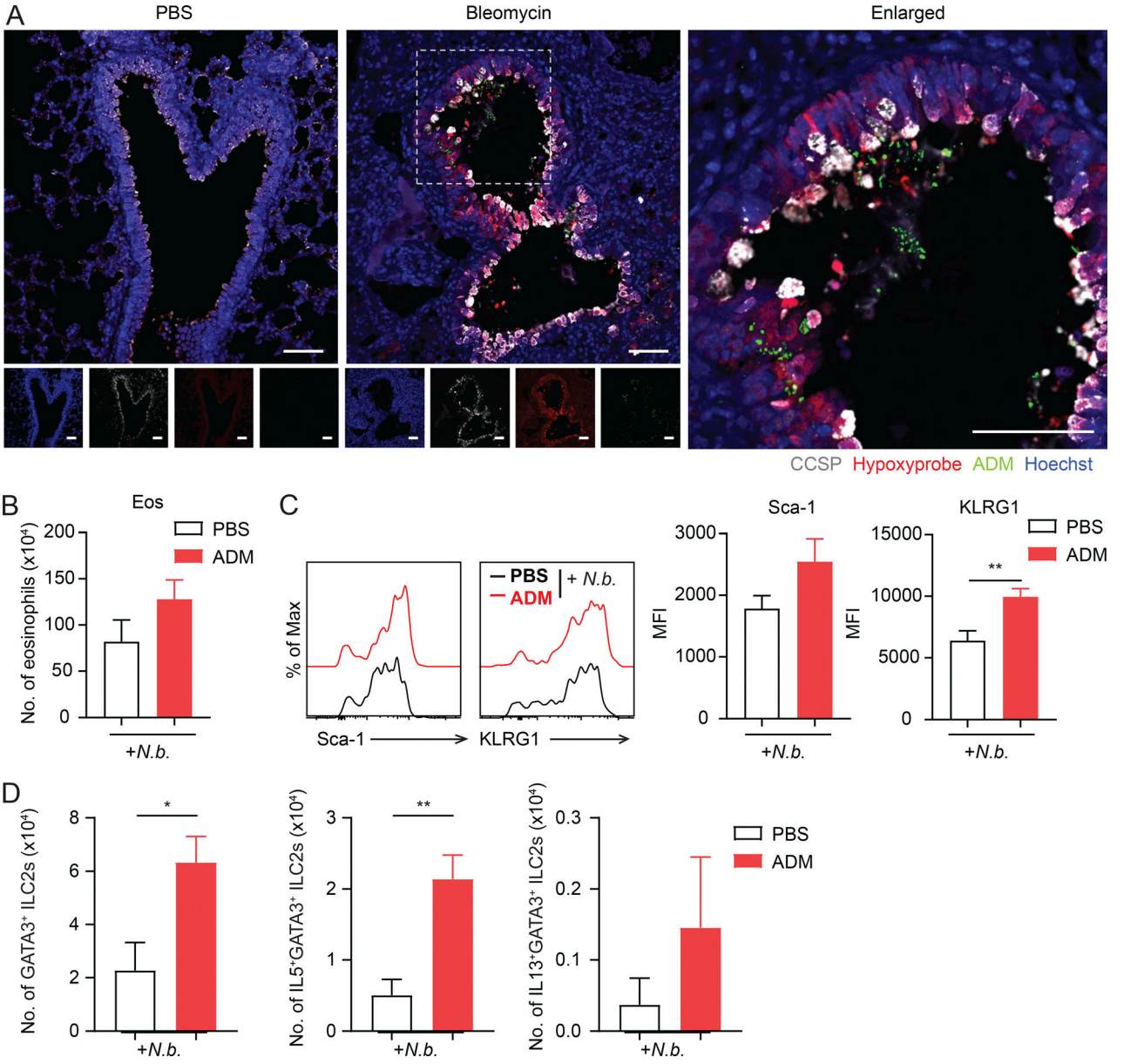

Figure S5. **Hypoxia-induced ADM elicits enhanced ILC2-mediated lung inflammation against helminth infection. (A)** Representative section of the lungs from WT mice after bleomycin instillation stained for CCSP (gray), hypoxyprobe-1 (red), ADM (green), and Hoechst (blue); 20× magnification; scale bars, 50 µm. White arrows highlight epithelial cells that show hypoxia; *n* = 2–3 mice/group. Data are representative of two independent experiments. **(B–D)** Lung cells from *N.b.*-infected mice were analyzed 2 d after infection. **(B)** The number of eosinophils in lung from PBS-treated or recombinant ADM-treated mice was determined by flow cytometry. **(C)** Flow cytometric analysis of expression (left) and quantification (right) of mean fluorescence intensity (MFI) of Sca-1 and KLRG1 in ILC2s. **(D)** The number of GATA3⁺ total ILC2s and IL-5– or IL-13–secreting ILC2s was counted after 4-h stimulation with PMA and ionomycin. Data are pooled from at least three independent experiments. Error bars indicate ± SEM. **(C and D)** *, P < 0.05; **, P < 0.01 (Student's *t* test).

Provided online are Table S1 and Table S2. Table S1 lists primers used for qPCR. Table S2 lists primers used for ChIP assay.